

LOW COST DYNAMOMETER SYSTEM TO
EXPERIMENTALLY MEASURE
PROPELLER PERFORMANCE
AT LOW REYNOLDS
NUMBERS

By

JOSEPH P. CONNER JR.

Bachelor of Science

Oklahoma State University

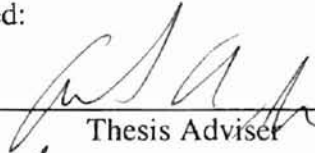
Stillwater, Oklahoma

1995

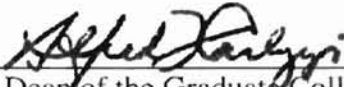
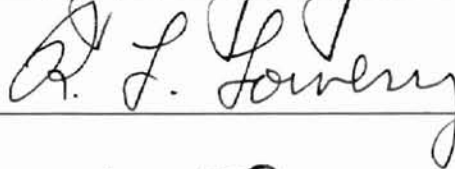
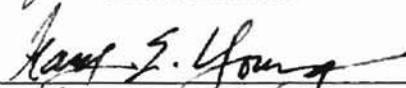
Submitted to the Faculty of the
Graduate College of the
Oklahoma State University
in partial fulfillment of
the requirements for
the Degree of
MASTER OF SCIENCE
December, 2000

LOW COST DYNAMOMETER SYSTEM TO
EXPERIMENTALLY MEASURE
PROPELLER PERFORMANCE
AT LOW REYNOLDS
NUMBERS

Thesis Approved:



Thesis Adviser



Dean of the Graduate College

ACKNOWLEDGEMENTS

I would first and foremost wish to express my thanks and appreciation to my major advisor, Dr. Andrew S. Arena, Jr., for his unending patience, constructive guidance, and his dedication and love to the field of teaching and research. I would also like to extend my thanks to my other committee members Dr. Gary Young, and Dr. Richard Lowery, whose guidance, encouragement and knowledge was an invaluable part of my education. I would also thank Mrs. Janet Smith for that special 'kick' that I needed when I was dragging my feet.

At this time I would like to take the time to thank all my friends for their support through out the years. A special thanks goes to Dr. Carlos Ize for all the help and encouragement given during all phases of the thesis and project.

A major thanks also goes to my parents for their support and guidance. They allowed me to grow and learn on my own, while still being there to help support me when I needed help, but more importantly to lend aid when I did not realize I needed help.

Finally I would like to thank all the Professors and staff members that I have worked with through out the years and for all the opportunities that they provided for to learn both in and out of the classroom.

"Failure is the opportunity to begin again, more intelligently" – Henry Ford

**"Not everything that can be counted counts,
and not everything that counts can be counted" --- Albert Einstein**

"Be EXCELLENT to each other" --- Bill and Ted

TABLE OF CONTENTS

Chapter		Page
1	INTRODUCTION	1
1.1	Problem Statement	1
1.2	Literature Review	2
2	THEORY.....	4
2.1	Propeller Aerodynamics	4
2.1.1	Thrust Coefficients	9
2.1.2	Torque and Power Coefficients	10
2.2	Aircraft and Propeller Combination Aerodynamics.....	12
2.2.1	Steady-Level Flight	12
2.2.2	Take-off Phase	16
3	EXPERIMENTAL APPARATUS	18
3.1	System Overview	18
3.2	Wind Tunnel Facility	19
3.3	Dynamometer.....	20
3.3.1	Torque.....	20
3.3.2	Thrust.....	24
3.3.3	Rotational Rate (RPS)	26
3.3.4	Support and Mount	28
3.3.5	Shroud.....	30
3.4	Electronic Components	31
3.5	Data Acquisition	34
4	EXPERIMENTAL PROCEDURE	36
4.1	Rational for Experimental Approach.....	36
4.2	List of Experiments Conducted.....	37
4.3	Calibration	37

Chapter		Page
4.3.1	Torque Sensor.....	37
4.3.2	Thrust Sensor.....	38
4.3.3	Rotational Rate.....	40
4.4	Data Acquisition and Processing.....	41
4.5	System Repeatability	43
4.6	Signal Quality.....	46
4.7	Uncertainty.....	55
5	EXPERIMENTAL RESULTS AND DISCUSSION	57
5.1	Reynolds number effect	57
5.2	Pitch sweep	60
5.3	Brand effect.....	63
5.4	Tip Clipping	66
6	CONCLUSIONS AND RECOMMENDATIONS	69
6.1	Conclusion	69
6.2	Recommendations.....	71
A	SOURCE CODES.....	74
A.1	PROPSCAN.CPP.....	74
A.2	D16.H	75
A.3	AIRPROPS.H.....	79
A.4	BITPRINT.H.....	80

LIST OF TABLES

Chapter	Page
TABLE 4.1 SAMPLE OF IMPORTED RAW DATA.....	43
TABLE 4.2 UNCERTAINTY OF MAJOR EQUATIONS.....	56

LIST OF FIGURES

Chapter	Page
FIGURE 2.1 EFFECT ON THE FOUR PROPELLER STAGES ON BLADE ELEMENT	6
FIGURE 2.2 CROSS SECTION EFFECTS ON WIND VELOCITY	7
FIGURE 2.3 SIMPLE BLADE ELEMENT GEOMETRY	9
FIGURE 2.4 STEADY-LEVEL FLIGHT FORCE DIAGRAM	13
FIGURE 2.5 STEADY-LEVEL MAXIMUM VELOCITY	15
FIGURE 2.6 TAKE-OFF PHASE FORCE DIAGRAM	16
FIGURE 3.1 SCHEMATICALLY OVERVIEW OF DYNAMOMETER SYSTEM	18
FIGURE 3.2: BASIC OVERVIEW OF WIND TUNNEL FACILITY	20
FIGURE 3.3 SKETCH OF OVERALL TORQUE SENSOR	21
FIGURE 3.4 SKETCH OF MOTOR MOUNT AND SHAFT	21
FIGURE 3.5 SKETCH OF SUPPORT SYSTEM AND WALLS	22
FIGURE 3.6 TORQUE SENSOR GAGE LAYOUT	23
FIGURE 3.7 SKETCH OF THE THRUST SENSOR	24
FIGURE 3.8 FORCE DIAGRAM ON A THRUST SENSOR LEG	25
FIGURE 3.9 THRUST SENSOR GAGE LAYOUT	26
FIGURE 3.10 STRAIN GAGE ALIGNMENT IN THE WHEATSTONE BRIDGE	26
FIGURE 3.11 SCHEMATIC OF ROTATIONAL RATE SENSOR	27
FIGURE 3.12 PLACEMENT OF ROTATIONAL SENSOR	28

Chapter	Page
FIGURE 3.13 SKETCH OF MAIN SUPPORT SYSTEM	29
FIGURE 3.14 SUPPORT FORMS	29
FIGURE 3.15 QUICK CONNECTION POINTS	30
FIGURE 3.16 CIRCUIT DIAGRAM OF WHEATSTONE BRIDGE	31
FIGURE 3.17 TORQUE/THRUST SUB-CIRCUIT DIAGRAM.....	32
FIGURE 3.18 ROTATIONAL RATE SUB-CIRCUIT DIAGRAM	33
FIGURE 3.19 INTERCHANGEABILITY OF ELECTRIC SYSTEM.....	34
FIGURE 4.1 CALIBRATION CURVE OF TORQUE SENSOR.....	38
FIGURE 4.2 CALIBRATION CURVE OF THRUST SENSOR	39
FIGURE 4.3 TARE DRAG OF DYNAMOMETER	40
FIGURE 4.4 REPEATABILITY TEST OF TORQUE COEFFICIENT.....	44
FIGURE 4.5 REPEATABILITY TEST OF THRUST COEFFICIENT	45
FIGURE 4.6 REPEATABILITY TEST OF PROPELLER EFFICIENCY	45
FIGURE 4.7 WAVEFORM OF THE THRUST SIGNAL AT 3600 RPM.....	46
FIGURE 4.8 WAVEFORM OF THE TORQUE SIGNAL AT 3600 RPM	47
FIGURE 4.9 WAVEFORM OF THE THRUST SIGNAL AT 4800 RPM.....	47
FIGURE 4.10 WAVEFORM OF THE TORQUE SIGNAL AT 4800 RPM	47
FIGURE 4.11 WAVEFORM OF THE THRUST SIGNAL AT 6000 RPM.....	48
FIGURE 4.12 WAVEFORM OF THE TORQUE SIGNAL AT 6000 RPM	48
FIGURE 4.13 SIGNAL TO NOISE RATIOS FOR TORQUE.....	49
FIGURE 4.14 SIGNAL TO NOISE RATIOS FOR THRUST	50
FIGURE 4.15 FFT FOR THRUST AT 120 RPS.....	51

Chapter	Page
FIGURE 4.16 FFT FOR TORQUE AT 120 RPS	51
FIGURE 4.17 FFT FOR THRUST AT 90 RPS.....	52
FIGURE 4.18 FFT FOR TORQUE AT 90 RPS	52
FIGURE 4.19 FFT FOR THRUST AT 60 RPS.....	53
FIGURE 4.20 FFT FOR TORQUE AT 60 RPS	53
FIGURE 4.21 (TORQUE) PERCENT ERROR BETWEEN AVG. VOLTAGE AND VOLTAGE RMS	54
FIGURE 4.22 (TORQUE) PERCENT ERROR BETWEEN AVG. VOLTAGE AND VOLTAGE RMS	54
FIGURE 5.1 REYNOLDS NUMBER EFFECT ON THRUST COEFFICIENT.....	58
FIGURE 5.2 REYNOLDS NUMBER EFFECT ON POWER COEFFICIENT	58
FIGURE 5.3 REYNOLDS NUMBER EFFECT ON PROPELLER EFFICIENCY	59
FIGURE 5.4 REYNOLDS NUMBER EFFECT ON THE RATIO OF THRUST AND POWER COEFFICIENT.....	59
FIGURE 5.5 PITCH EFFECTS THRUST COEFFICIENT	61
FIGURE 5.6 PITCH EFFECTS ON POWER COEFFICIENT	61
FIGURE 5.7 PITCH EFFECTS ON THE PROPELLER EFFICIENCY	62
FIGURE 5.8 PITCH EFFECTS ON THE RATIO OF THRUST AND POWER COEFFICIENTS	62
FIGURE 5.9 DIFFERING BRAND EFFECTS ON THE THRUST COEFFICIENT	64
FIGURE 5.10 DIFFERING BRAND EFFECTS ON THE POWER COEFFICIENT	64
FIGURE 5.11 DIFFERING BRAND EFFECTS ON THE PROPELLER EFFICIENCY	65
FIGURE 5.12 DIFFERING BRAND EFFECTS ON THE RATIO OF THRUST AND POWER COEFFICIENT	65
FIGURE 5.13 TIP CLIPPING EFFECTS ON THE THRUST COEFFICIENT	67
FIGURE 5.14 TIP CLIPPING EFFECTS ON THE POWER COEFFICIENT.....	67

Chapter	Page
FIGURE 5.15 TIP CLIPPING EFFECTS ON THE PROPELLER EFFICIENCY	68
FIGURE 5.16 TIP CLIPPING EFFECTS ON THE RATIO OF THRUST AND POWER COEFFICIENT	68

NOMENCLATURE

C	Chord length
C_D	Drag Coefficient
C_L	Lift Coefficient
C_P	Power Coefficient
C_Q	Torque Coefficient
C_T	Thrust Coefficient
d	Diameter
D	Drag Force
F_n	Normal Force
g	Acceleration of Gravity
J	Advance Ratio
L	Lift Force
N	Rotational Rate (revs per sec)
m	Mass of the Aircraft
P, p	Pitch (inches)
Q	Torque Measured (oz-in)
r	Station Radius
R	Blade Radius (inches)
RPM	Revolutions per Minute
S	Wing Surface Area
T	Thrust Measured (oz)
V	Airspeed Velocity (ft/sec)
V_r	Rotational Velocity (rad/sec)
W	Total Weight of the Aircraft
α	Blade Section Angle of Attack
β	Blade Angle
η	Propeller Efficiency
μ	Friction Coefficient
π	Pi
ρ	Density of Air

CHAPTER I

1 INTRODUCTION

1.1 Problem Statement

One of the more difficult jobs in designing remotely piloted vehicles (RPV) is the selection of the propeller for a given propulsion system. This is largely due to the lack of accurate propeller performance curves. This lack of information leads to a need for the development of a system to accurately measure all the valuables that govern a propeller's performance.

The system developed can simultaneously measure and record the propeller's thrust, torque, and rpm. This is done by use of a custom-built instrumentation and a data acquisition system. The thrust and torque coefficient as well as overall propeller efficiency can then be found from the recorded propeller measurements.

The rotational rate of the propeller is found by use of an infrared emitter and detector. The infrared light is emitted onto the back of the spinner, where a thin aluminum disk is mounted. The disk is painted black except for a small arced area. This section is polished so that it will reflect the light, emitted from the emitter, back into the detector. The signal that is produced from the rotation of the disk is then sent into a comparator circuit, resulting in a TTL signal.

Thrust is found by use of measuring the strain produced by the deflection of two thin beams, which support the entire device. The torque is also measured by the strain produced in the twisting of a two-beam cruciform that is attached to a shaft. The shaft is then connected to the rear of the motor mount. The strain that is produced in both cases is

measured by use of strain gages that are attached directly to the beams. The strain gages are then connected to in a circuit to form a full Wheatstone bridge, where the output voltage corresponds to the thrust and torque placed upon the system. This voltage is then recorded on the computer by use of a data acquisition card and program. The power that is provided by the power supply is also monitored and recorded to aid in determining the overall system efficiency.

The entire system can be mounted inside the low-speed wind tunnel, located at the Aerodynamics laboratory at Oklahoma State University. This dynamometer and wind tunnel test section, will allow tests of propellers in either a 'tractor' or 'pusher' configuration as well as tests over a large range of propeller diameter, pitch, and airspeeds.

1.2 Literature Review

As of date of this thesis, there have been few papers that have address the issue of experimental determining the dynamic performance of small scale propellers in the low Reynolds number regime. In fact there are few papers that address the issue of testing of any kind for propellers below a meter in diameter. Asson (1990) developed did develop a dynamometer that could test small size propellers and determine the propeller performance to with in $\pm 5\%$ error, however this system was costly and was limited to rotational speeds below 1000 RPM. Takasawa and Hashidate (1990) also developed a low-Reynolds number dynamometer that showed good results, however this system was designed to test a propeller that had been develop for a microwave-powered airplane that had a propeller in the range of two and half meters in diameter.

Hurst, Methven, and Owen (1986) describe a system that can drive a propeller up to 10,000 RPM, and determines its performance by use of a Scanivalve system connected to 24 chordwise tapings positioned at 7 spanwise blade locations. This pressure distribution can then be transferred to thrust and torque coefficients. One of the more interesting papers was by Harrison (1987) and involves the use of a laser Doppler velocimetry system that can be used to determine the velocity field around a 12" diameter counter rotating propeller configuration. Schetz, Mallory and Pelletier (1987) also measured the velocity and pressure distributions in the wake of a 19.5" diameter propeller using a hot-wire anemometer. Unfortunately each of the system that do not directly measure the torque and thrust are very hard to adapt to a new arrangement and also can lead to a large scattering of data.

CHAPTER II

2 Theory

2.1 Propeller Aerodynamics

The propeller is defined as a device for producing thrust at normal forward velocities of the aircraft. From this definition one can see that the prime output of a propeller is thrust. The propulsion system engineer must determine an overall power system that will produce a maximum thrust under all expected conditions. The main problem that one faces is that the combination of airplane, engine, power supply, and propeller is interconnected so that one must evaluate the entire system as one.

The propeller develops thrust by changing the rotational motion of the motor to forward motion. One simple mechanical device that can behave in the same manner is a machine screw. The screw uses threads to push back on the surrounding surface to move forward, this is one of the reasons that a propeller is also called an airscrew. The airscrew pushes backward on the surrounding air, which in turn causes it to move forward. A propeller, like a machine screw also, has a pitch. The only major difference is that a propeller has two types of pitch; geometric and effective. Geometric pitch is the theoretical advance per revolution of a propeller blade as it moves along a helix whose angle equals the propeller blade angle. Effective pitch is the distance the propeller and aircraft actually move in a single revolution. The difference between the two types of pitch is called slip and this slip will vary with forward speed.

$$p = \pi d \tan \beta \quad (2.1)$$

Most propellers can be placed into three categories: fixed pitch, adjustable pitch, and controllable pitch. Fixed pitch is a propeller that is constructed as one piece and in which the pitch, or blade angle, cannot be altered after construction. Adjustable pitch is a propeller that is constructed in such a manner that one can adjust the blade angle to a desired setting on the ground, after the adjustment the 'new' blade angle is fixed in flight. Controllable pitch is a propeller that will allow one to change the blade angle in flight. The change can be controlled manually or automatically during flight to maintain a given power load.

The propeller's performance can be broken down into four stages: fan, propeller, brake, and windmill stages. The fan stage is encountered when the forward velocity of the propeller is zero, the next stage that a propeller will encounter is the propeller stage. The propeller stage is simply a region in which the blade produces a positive thrust, after this 'productive' thrust stage a region of negative thrust is encountered. This region of negative thrust is called the brake stage. During this phase the thrust actually furnishes additional drag to the aircraft, one important thing is that the torque to the propeller is still positive. The final phase is the windmill stage, in this stage not only is the thrust negative but aerodynamic forces acting on the propeller actually produce torque which is feedback into the motor. The majority of the time a propeller operates in the propeller stage, however the other stages are also important to understand. Static thrust occurs in the fan stage and is an important factor in the determination of the aircraft's takeoff qualities. Braking and wind milling can only be readily encountered in a power dive and both of these stages need to be avoided as they can lead to damage of the motor. All four

of the stages are readily visualized in Figure 2.1 with use of the simple blade element theory (Nelson 1944).

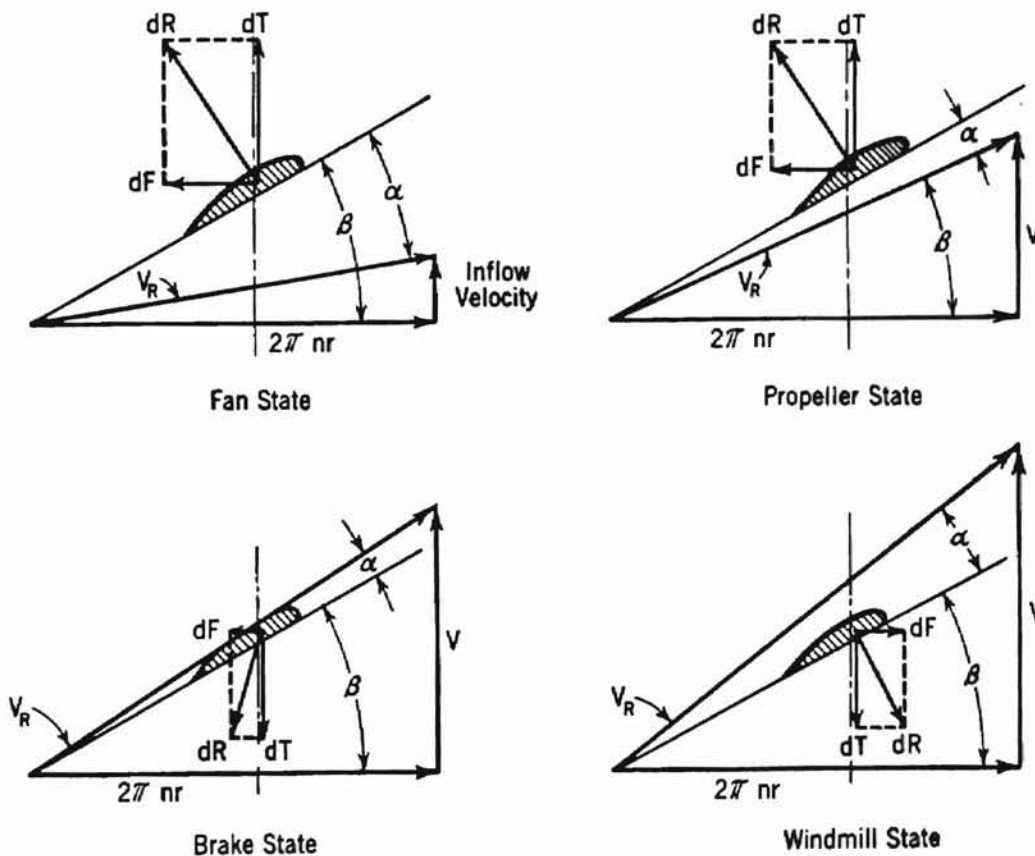


Figure 2.1 Effect on the four Propeller stages on Blade Element

The propeller can be examined as a wing with very large amounts of twist. If one was to examine a cross section of a propeller blade they would see that it is essentially the same shape as that of a wing. However, propeller sections usually have a greater thickness ratio than an airfoil. This increase in thickness can be even more evident in some brands as the blade sections approach the hub. Although there is a difference in thickness ratio between a blade and airfoil section, the major differing factor that contributes to the geometric difference between the two is the orientation of a blade section profile changes considerably as the sections proceed from the tip inward toward

the hub. This change in blade angle is to account for the different wind velocity that each blade section will see. This variance in wind velocity is mainly caused by the rotation of the blade. For a wing the magnitude and direction of the wind velocity is essentially the same along the entire span of a wing. Whereas, in the case of the propeller, the magnitude and direction of the wind velocity vary across the span of the blade. This change in wind velocity is twofold: The propeller is moving with the forward motion of the wing and it rotates about its own axis. Under most conditions the direction of this axis of rotation and the forward motion may be considered aligned. Therefore a given blade section has a velocity component in the direction of flight and a rotational velocity component which is perpendicular to the axis of rotation, or the propeller axis. The wind velocity that each blade section sees is then the resultant of both the forward and rotational components of velocity. In Figure 2.2 the effect of this change can be seen at three blade cross section.

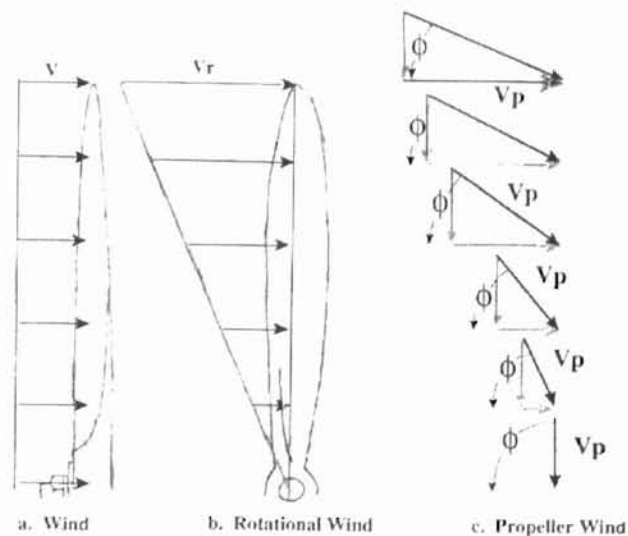


Figure 2.2 Cross section effects on wind velocity

It should be apparent that the forward velocity is a constant for the entire span of the blade, while the rotational velocity will change along the span of the blade. This change in rotational velocity is proportional to the distance from the propeller axis. The rate at which the propeller rotates can be given as either; the number of revolutions per second or the angular velocity. The angle ϕ between the rotational velocity component and the forward velocity can be found with the equation:

$$\tan \phi = \frac{V}{r\omega} = \frac{V}{2\pi nr} = \frac{V}{\pi nd} \quad (2.2)$$

With this equation, it can be seen that the angle ϕ will decrease with an increase of radial position r . Since the blade angle β can be defined as the angle between the blade chord line and the plane of rotation, the effective angle of attack for a given section will be:

$$\alpha = \beta - \phi \quad (2.3)$$

The dimensionless quantity V/nd is called the advance ratio of the propeller. This ratio allows geometrically similar propellers to be compared to each other as the angle of attack of each corresponding blade section will be the same value. This will hold if and only if the corresponding blade sections have the same shape, orientation and the advance ratio is the same for both propellers. The advance ratio for a given blade angle can be thought of as analogous to the angle of attack in airfoil tests, and it is therefore customary to plot the propeller performance curves versus the advance ratio. In order to determine the thrust and torque produced in geometrically similar propellers it is necessary to reduce the thrust and torque to some form of coefficient.

2.1.1 Thrust Coefficients

The propeller thrust produced acts along the axis of rotation and is the primary product of interest, as this is the force that will propel the aircraft forward. From the Simple Blade Element Theory (Nelson 1944), which is graphically shown in Figure 2.3,

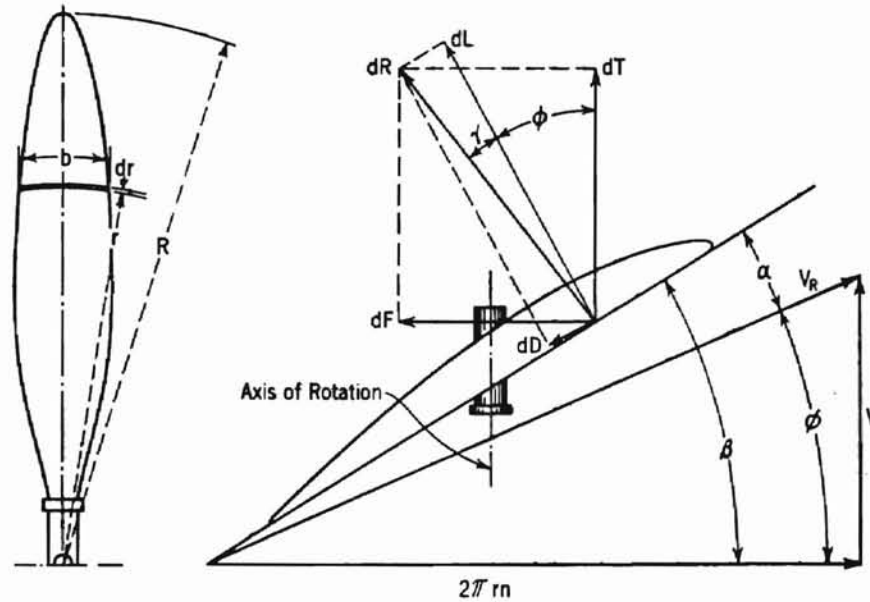


Figure 2.3 Simple Blade Element Geometry

the expression for thrust is:

$$dT = \frac{1}{2} \rho V^2 b dr C_L \left[\frac{\cos(\phi + \gamma)}{\sin^2 \phi \cos \gamma} \right] \quad (2.4)$$

Since both b and r vary directly with diameter for geometrically similar propellers, and the angles ϕ and γ as well as C_L are all dependent on the advance ratio only, the expression for thrust can then be simplified for a given advance ratio to:

$$T = C_T \rho V^2 d^2 \quad (2.5)$$

This can then be rearranged into a thrust coefficient of the form:

$$C_T = \frac{T}{\rho V^2 d^2} \quad (2.6)$$

Since this form contains forward velocity a coefficient for the windmill stage, or static condition, can not be determined since the result will be a coefficient approaching infinity. In order to determine the static thrust, and thus takeoff performance, the equation must be rearranged in such a manner to remove the velocity. This is done by multiplying the equation by the advance ratio with the proper power so as to eliminate the velocity. Once this has been done the thrust coefficient now has the form:

$$C_T = \frac{T}{\rho n^2 d^4} \quad (2.7)$$

This form will now allow the static condition to be determined. While the thrust coefficient will allow one to determine the thrust produced, this is only a part of the overall picture.

2.1.2 Torque and Power Coefficients

Unfortunately power must be put into the propeller in order for it to rotate, this power requirement comes from the torque that is required in order to overcome both the inertia and aerodynamic forces acting on the propeller. As was seen in Figure 2.3 the lift produced by a blade section not only has a component perpendicular to the plane of rotation, but it also has a component parallel to the plane of rotation that opposes the rotation of the propeller. The drag produced by a blade section also has components that not only oppose the rotation of the propeller, but it also has a component that is perpendicular to the plane of rotation. Unfortunately this component of drag acts in the opposite direction as the forward motion of the aircraft and as such opposes the thrust

that is being produced. With use of the Simple Blade Element Theory, an expression for the torque is found to be:

$$dQ = \frac{1}{2} \rho V^2 b r dr C_L \left[\frac{\sin(\phi + \gamma)}{\cos \gamma \sin^2 \phi} \right] \quad (2.8)$$

The expression for torque can then be simplified for a given advance ratio by the same method used for the thrust.

$$Q = C_Q \rho V^2 d^3 \quad (2.9)$$

This can then be rearranged into a torque coefficient of the form:

$$C_Q = \frac{Q}{\rho V^2 d^3} \quad (2.10)$$

This form is then rearranged in a similar fashion to the thrust coefficient in order to eliminate the forward velocity. Once this has been done the torque coefficient now takes on the form:

$$C_Q = \frac{Q}{\rho n^2 d^5} \quad (2.11)$$

Now that a torque coefficient has been found, a power coefficient may be derived using the relationship that power is directly proportional to the torque and the rotational rate:

$$C_P = \frac{2\pi n Q}{\rho n^3 d^5} = \frac{P}{\rho n^3 d^5} \quad (2.12)$$

With an expression for both thrust and power coefficients having been found, an expression for the propeller efficiency can now be derived. The propeller efficiency will

allow one to find the propeller power out that is produced for a given shaft power. The power that is transmitted into the propeller shaft is a product of the torque and resulting angular velocity, where as the propeller power produced is a product of thrust and the velocity. This results in:

$$\eta = \frac{TV}{2\pi nQ} = \frac{TV}{P} \quad (2.13)$$

This equation can then be rearranged with use of equations (2.7) and (2.12):

$$\eta = \frac{C_T \rho n^2 d^4 V}{C_P \rho n^3 d^5} = \frac{C_T}{C_P} \frac{V}{nd} \quad (2.14)$$

2.2 Aircraft and Propeller Combination Aerodynamics

With expressions for both the power and thrust coefficients now found, one can look at the amount of power the entire aircraft will require during each phase of flight. The two most important phases of flight that will be looked at here are the steady level phase of flight as well as the take-off phase.

2.2.1 Steady-Level Flight

The steady-level phase of flight in general is characterized by flight in a vertical plane that at small flight path angles, relatively small changes in the airspeed, and small changes in altitude. To develop the governing equations for this phase of flight, the diagram as shown in Figure 2.4 is used to balance the forces.

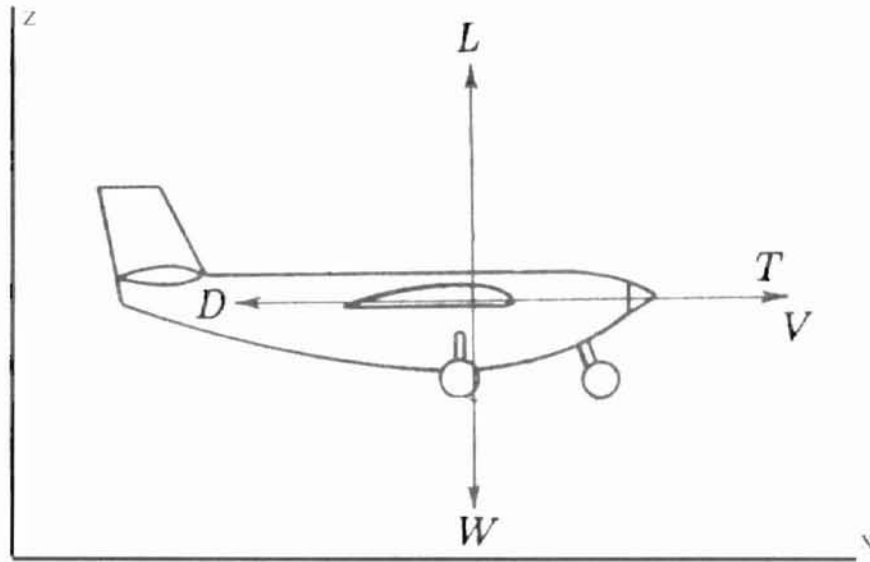


Figure 2.4 Steady-Level Flight Force Diagram

From this we can develop the following equations;

$$mg = \frac{1}{2} \rho S V^2 C_L \quad (2.15)$$

and

$$T = \frac{1}{2} \rho S V^2 C_D \quad (2.16)$$

Equation (2.15) is the lift equation and indicates the lift that force must be produced in order for level flight. The next equation (2.16) is the thrust equation, this equation indicates how much thrust the propeller must deliver to the air stream in order that the aircraft be able to move through the air at a steady rate. It is this second equation that will be used to determine the amount of power that must be provided by the propeller to the air stream. In order to determine the amount of power that must be provided, both

sides equation (2.16) must be multiplied by the air stream velocity. This results in the following equation:

$$TV = \frac{1}{2} \rho S V^3 C_D \quad (2.17)$$

The left-hand side of equation (2.17) is the amount of power that is provided to the air stream by the propeller and motor. The right-hand side is the amount of power that is required to overcome the drag force on the aircraft. Since the thrust provided by the propeller can be found with use of the thrust coefficient, equation (2.7), equation (2.17) can be rewritten in the form:

$$C_T \rho n^2 d^4 V = \frac{1}{2} \rho S V^3 C_D \quad (2.18)$$

One can now rearrange equation (2.18) into a form that solves for the thrust coefficient required to overcome the drag coefficient of the entire aircraft. This results in:

$$C_T = \frac{S V^3 C_D}{2 n^2 d^4} \quad (2.19)$$

Which can then be simplified with the substitution of the advanced ratio to produce an equation that for a given aircraft will result in a required thrust coefficient that can be solved as a function of only the diameter of the propeller over a given advanced ratio range.

$$C_T = \frac{S J^2 C_D}{2 d^2} \quad (2.20)$$

This now allows the designer a tool to determine the steady-level velocity of the aircraft for a given propeller. To do this one must plot the thrust coefficients of varying P/D ratios versus a fixed diameter and advance ratio. The point of intersection on this plot indicates the velocity at which the aircraft can reach with the given propeller. A sample of the type of results that are produced are shown in Figure 2.5

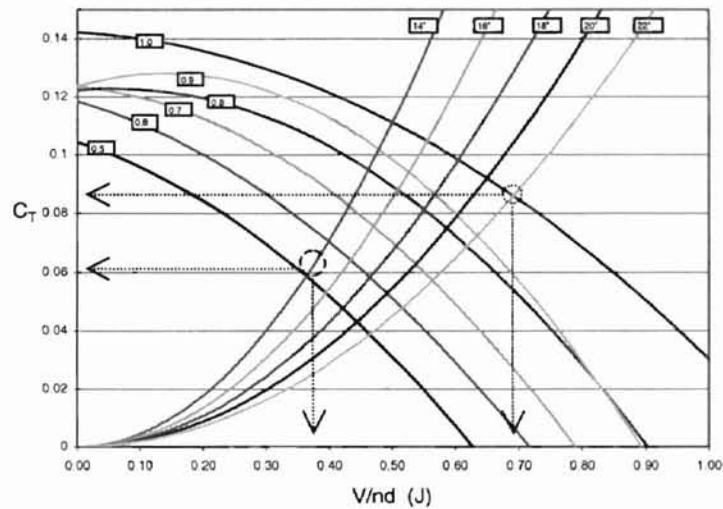


Figure 2.5 Steady-Level Maximum Velocity

While this will aid the designer in determining the top level speed of the aircraft, it does not really provide the required information as to the power that is required for the aircraft to actually get in the air. In order to determine the amount of power required for the aircraft to take-off, one must analyze the forces which must be overcome during this phase. The phase must be analyzed for the simple fact that if the aircraft can not obtain the power required for take-off, it will never be able to reach the steady-level phase of flight.

2.2.2 Take-off Phase

The take-off phase of flight is characterized as the time from which the aircraft is stationary on the ground to a point where the aircraft has accelerated to a velocity significant for flight. It is this acceleration of the aircraft to flight speed that will determine the amount of power that is used. In order to determine the amount of acceleration required for the aircraft to take-off with in its given design restrains, we will look at the equations of motion which apply to the aircraft during this phase.

In order to develop the governing equations for take-off, Figure 2.6 will be used to aid in the balancing of the forces and accelerations.

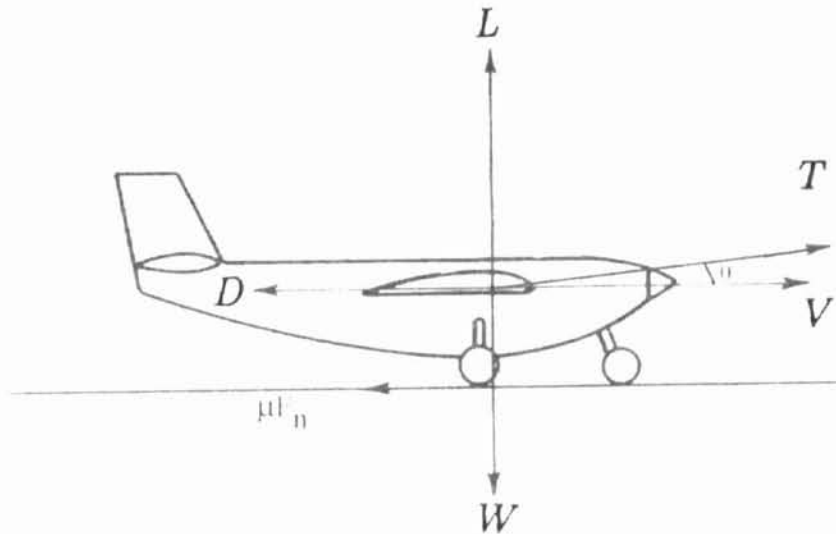


Figure 2.6 Take-Off Phase Force Diagram

From this we can develop the following equation:

$$F = ma = T \cos \theta - D - \mu F_n \quad (2.21)$$

However one must also recall that since the aircraft does produce lift as it rolls down the run-away, the normal force that is produced by the aircraft varies as a function of velocity. Therefore the normal force (F_n) can be expressed as follows:

$$F_n = W - L - T \sin \theta \quad (2.22)$$

This can now be substituted back into equation (2.21) and will result in the total net acceleration of:

$$F = ma = C_T \rho n^2 d^4 \cos \theta - \frac{1}{2} \rho S V^2 C_D - \mu \left(mg - \frac{1}{2} \rho S V^2 C_L - C_T \rho n^2 d^4 \sin \theta \right) \quad (2.23)$$

Now with the net acceleration on the aircraft found, we can find the total distance that will be required for the aircraft to travel until the velocity reaches a level that allows the lift force to exceed the weight force. As can be seen from this chapter, the designer needs some way to determine the thrust and power coefficients of the propeller. In order to do this a custom dynamometer has been designed and built to accomplish the task of determining the dynamic performance of a propeller that is required for the design.

CHAPTER III

3 EXPERIMENTAL APPARATUS

3.1 System Overview

To correctly determine the dynamic performance of a propeller, one must be able to actually measure the power in and power out. The power out can be found by measuring the thrust and the tunnel velocity, and the power in is found by measuring the torque on the motor as well as the rotational rate of the propeller. To accomplish this task an effective way had to be found to simultaneously measure the torque, thrust, rotational rate of the propeller as well as the tunnel velocity. A schematic overview of the final dynamometer is shown in Figure 3.1.

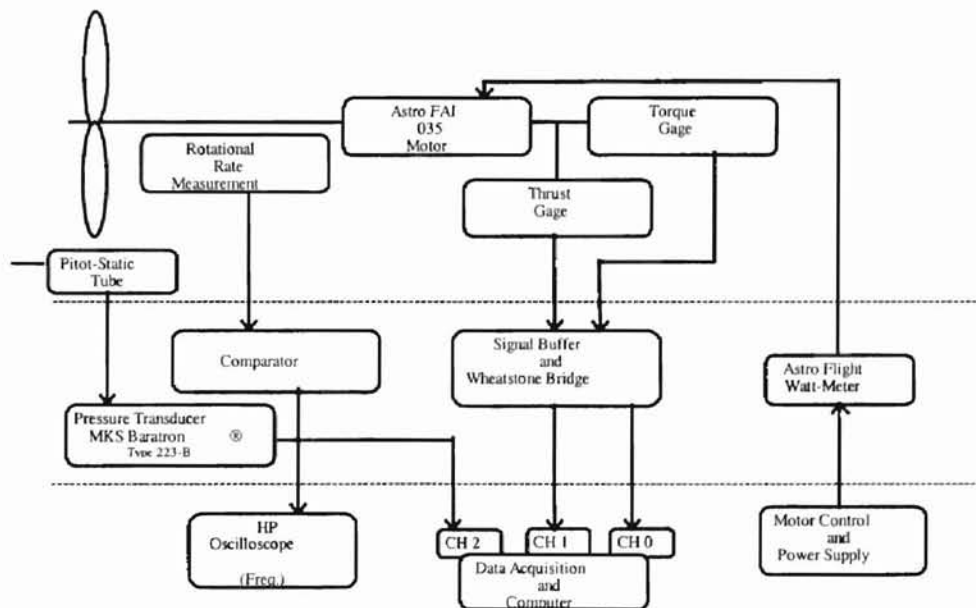


Figure 3.1 Schematic Overview of Dynamometer System

The entire dynamometer system is composed of the mechanical and electrical sensors that are housed in the actual dynamometer, which is mounted in the wind tunnel

test section, the external signal conditioning and power control units, an IBM 386 utilized for data acquisition, and the wind tunnel with related equipment.

3.2 Wind Tunnel Facility

The experiments were conducted in the wind tunnel located in the Aerodynamics lab at Oklahoma State University. The tunnel is powered by a 125 hp AC motor, which drives the flow through anti-turbulence screens, the contraction section, the interchangeable test section, and diffuser. The contraction cone at the inlet has a 15 to 1 contraction ratio. The diffuser section attaches to an interchangeable test section, which has the three foot cross section installed for this setup of experiments. The test section then connects to a section which diverges through an angle of 5.6° to a circular radius where the fan is located. Behind the rectangular-circular transformation section is a circular straw box consisting of common drinking straws which are aligned with the flow to reduce any disturbances caused by the fan or atmospheric conditions downstream of the fan section.

To determine the conditions inside the test section, a pitot-static tube and an inclined manometer are used to measure the dynamic pressure and a thermocouple is used to determine the temperature inside the wind tunnel. A barometer is used to resolve the local barometric pressure. An overview of the wind tunnel facility is illustrated in Figure 3.2.

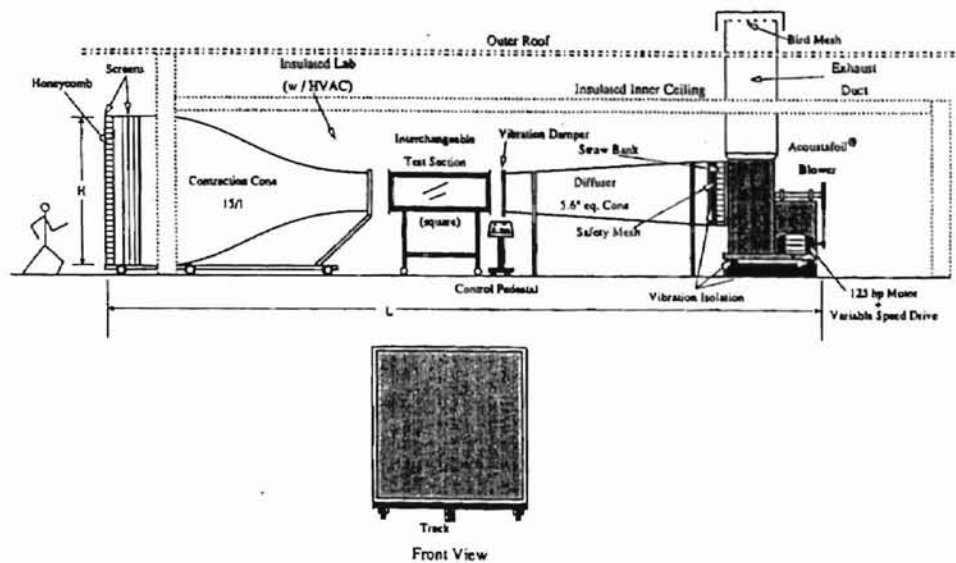


Figure 3.2: Basic Overview of Wind Tunnel Facility

3.3 Dynamometer

3.3.1 Torque

In order to avoid the complexities of a torque sensor with a separate propeller shaft and bearing system, the propeller is mounted directly on the motor. The motor itself is then attached directly to a solid steel shaft. This shaft then transfers the torque produced on the shaft to a two beam cruciform, the strain is then measured by strain gages which are attached to the legs of the cruciform then measure the strain produced by this load. A diagram of the torque sensor as a system is shown in Figure 3.3

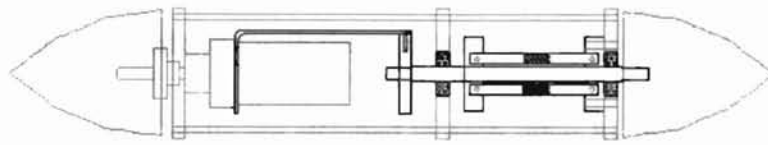


Figure 3.3 Sketch of Overall Torque Sensor

The motor is mounted directly to a thin aluminum motor mount. This motor mount is then attached to a steel shaft by means of a small Plexiglas spacer. This spacer has two 0.25" diameter holes in it. The two hole allow both direct and geared motors to be tested, as the holes are aligned in such that the line of action is aligned with the center line of the steel shaft. The steel shaft was a solid 0.375" diameter rod that has been turned down to 0.3125" along the length of the shaft. The ends of this shaft were then turned and then a threaded to $\frac{1}{4} \times 20$, this allows the attachment of the motor mount as well as a rear fairing.

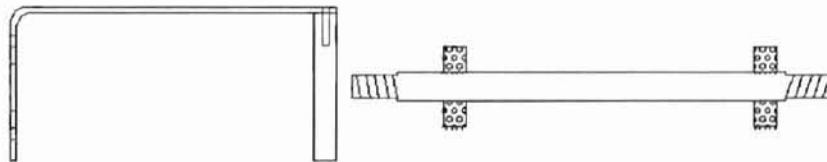


Figure 3.4 Sketch of Motor Mount and Shaft

The shaft is supported by two Plexiglas walls, these walls are 2.6" in diameter and 0.25" in thickness. In the center of both of these walls a bearing has been located, this bearing has an inside radius of 0.3125" and thus is the main reason the shaft had to be turned to this size. There is also a third Plexiglas wall, this wall is also 2.6" in diameter but

this wall has a 1.8" diameter hole placed in the center. This allows the motor shaft to rotate freely with out interfering with the support wall.

All three of these walls are attached to each other by means of a 10-28 all-thread steel rod. The walls are held in place but nuts which are securely drawn up next to each wall. This support system allows the shaft to freely rotate. To measure the amount of twist and thus torque being applied to the shaft, a two beam cruciform is attached to the top of the shaft.

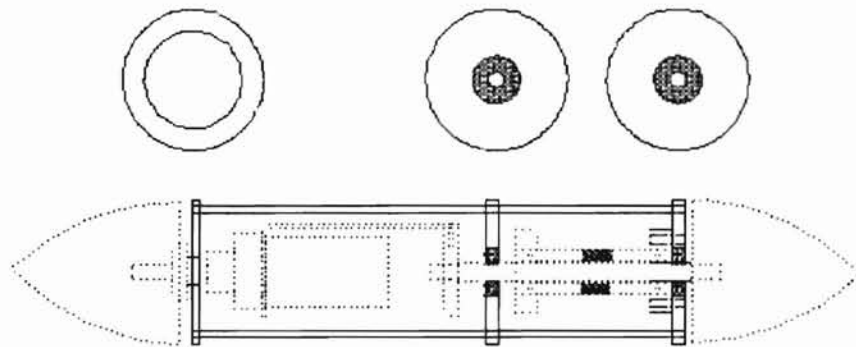


Figure 3.5 Sketch of Support System and Walls

This cruciform is rigidly attached to the shaft at the end nearest to the motor, the opposite end is allowed to float above the shaft. This end of the shaft however is then rigidly attached to the rear Plexiglas wall. This configuration allows the shaft to twist the cruciform at one end while the opposite end is held in place relative to the rear support wall. This twist produces a strain in the legs of the cruciform. This strain is measured by means of four strain gages that have been attached directly to the legs of the cruciform. The pattern in which the gages have been layout out is shown in Figure 3.6.

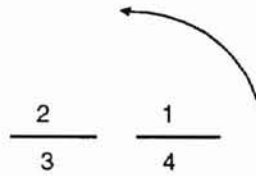


Figure 3.6 Torque Sensor Gage Layout

This pattern allows for full temperature compensation and also increases the sensitivity by a factor of two.

The cruciform itself is constructed from one solid piece of aluminum. This piece was milled as one piece to insure that the load transmitted from the attachment point was properly transmitted to the legs. The cruciform was made with several machining operations. The first operation that was done to mill a 0.3125" radius channel down the middle of the entire piece. After this was done, the channel was then enlarged by 0.1" along the piece with the exception of the end where the shaft would be attached to the cruciform. This enlargement of the channel was done to ensure that the shaft only made contact with the cruciform at the desired location. After completion of the center channel was completed the piece was turned over and the operation to create the legs was started, this operation involved milling the legs down to a thickness of 0.0625". The next step was to mill the legs to the desired width of 0.200", this process involved the removal of material from the outside of the legs.

After this was done the attachment holes were drilled. The shaft attachment hole was drilled to allow number 6 bolt to pass though the cruciform and then aligned with a thread that was placed in the center of the shaft. This attachment rigidly secures the forward end of the cruciform and the shaft. The opposite end then had two holes drilled

through it and the end support wall. A bolt is then passed through this hole where a washer and nut is attached to secure this end of the cruciform to the wall.

3.3.2 Thrust

It was decided to use simple beam deflection to measure the thrust that is produced by the propeller. This decision was made for two reason; first since the dynamometer needed to be placed in the center of the test section so this lead to the need for some type of support. Second, the beam deflection method avoided the complexities of a spring and LVDT that have been used by others. The torque sensor and support system are mounted directly to the top of a double beam. An overall diagram of the thrust sensor can be seen in Figure 3.7

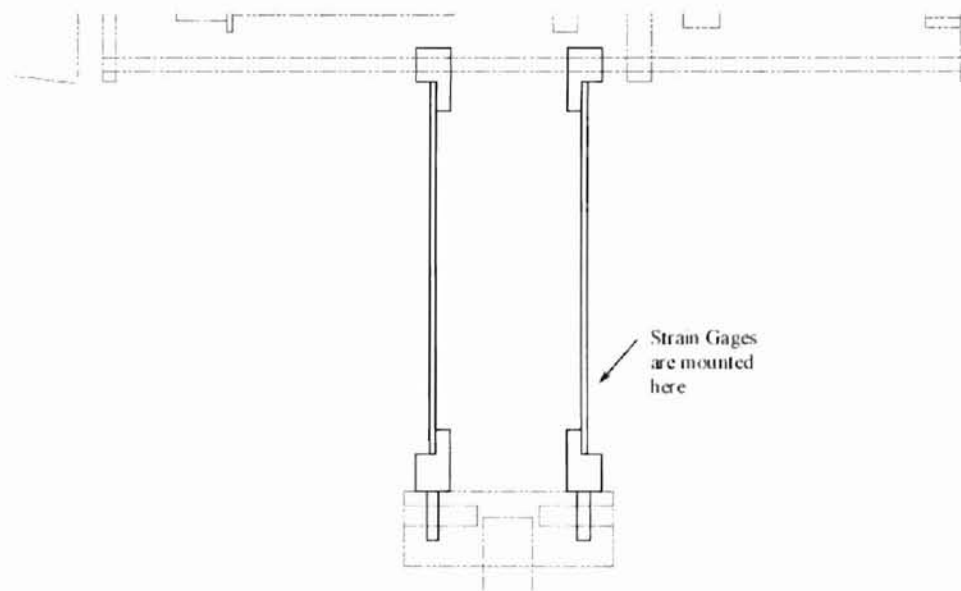


Figure 3.7 Sketch of the Thrust Sensor

The system is mounted on top of two thin aluminum legs, the legs have been milled to a thickness of 0.065" and a length of 3.8". The legs are then attached to a solid

aluminum piece that has been milled to allow the legs to be mounted perpendicular to each other. In order to allow the top of the sensor to be mounted as near its center of gravity, the top of the legs have an attachment that allows adjustment of the position of the interface between the legs and the torque sensor. This arrangement allows only an active beam length of 3.7". A simple diagram of how the thrust sensor works is shown in Figure 3.8

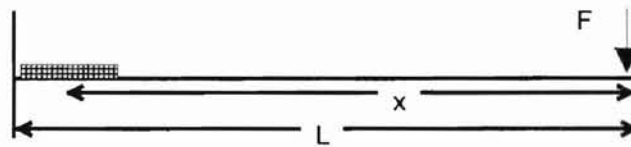


Figure 3.8 Force Diagram on a Thrust Sensor Leg

To insure that the maximum bending stress is measured, therefore allowing maximum mechanical sensitivity, the strain gages are located at the base of the legs. In order to make the most of the maximum sensitivity, four gages are installed at the base of one leg. The pattern in which the gages have been attached to the leg are shown in Figure 3.9

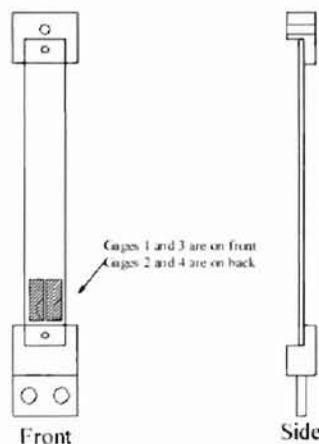


Figure 3.9 Thrust Sensor Gage Layout

This arrangement of strain gages allows for full temperature effects, as well as axial and torsional components are all compensated for, as well an increase in the sensitivity by a factor of four. One other benefit is that this system of strain gages allows the use of a four-arm bridge. The four-arm bridge is actually the base of a wheatstone bridge that is used to measure the strain that is measured by the gages. The arrangement of the sensors in the wheatstone bridge are shown in Figure 3.10

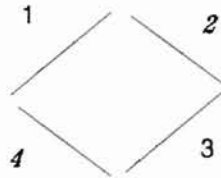


Figure 3.10 Strain Gage Alignment in the Wheatstone Bridge

3.3.3 Rotational Rate (RPS)

The rotational rate of the propeller was found by use of an infrared emitter and detector. The infrared light was emitted onto the back of the spinner, where a thin aluminum disk was mounted. The light emitted from the emitter is then reflected back into the detector. A schematic of this sensor is shown in Figure 3.11

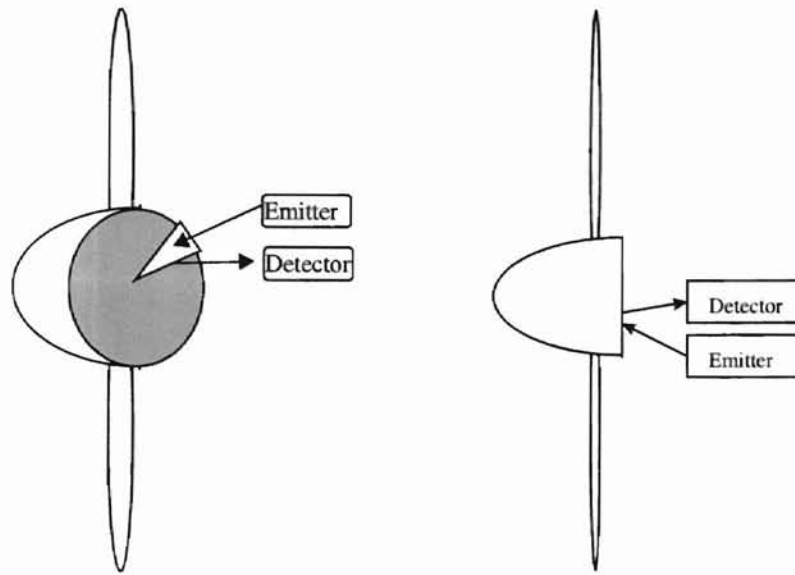


Figure 3.11 Schematic of Rotational Rate Sensor

The spinner back plate is attached directly to the motor shaft, the plate is held in place by the propeller and a nut. A thin aluminum ,0.027" thickness, disk was cut to a radius of 2.5" to match the size of the spinner plate. It is attached to the rear of the spinner plate with a thin foam padding to fill the gap between the rear of the spinner plate and the aluminum disk. The aluminum disk is paint a flat black with the exception of a small 25° arc, which was then polished to be highly reflective. This small reflective arc has a much higher reflective rate then the flat black zone and thus allows the measurement when this area passes in front of the sensor array.

The sensor array consists of a high power infrared emitter and an independent infrared detector. The two are mounted in the forward support wall, with the detector on the inner radius. To support the sensors two small holes have been drilled into the forward support wall (Figure 3.12). The sensors are then plugged into a modified 8-pin socket which allows them to interface with the electric system.

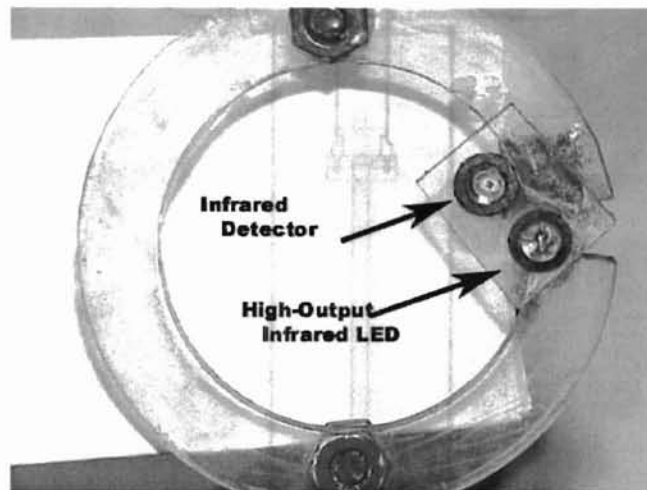


Figure 3.12 Placement of Rotational Sensor

The signal that is produced by the rotation of this disk is then sent to a comparator circuit, resulting in a TTL signal instead of the 'spike' produced in the raw signal. This signal allows an easier detection of the frequency, which corresponds directly to the rotational rate of the propeller shaft.

3.3.4 Support and Mount

The dynamometer is supported on top of a 1/2" diameter steel rod. This rod solved two major problems. One alignment of the dynamometer with the center line of the tunnel, and also it allowed the dynamometer to be supported 1.5 ft while maintaining the needed stiffness. This rod has been threaded on the top so that the dynamometer can be attached to the rod and then had been press fitted into a steel plate support. This steel plate is held in place on the tunnel floor by means of 4 bolts. A super structure is then attached over the steel rod.

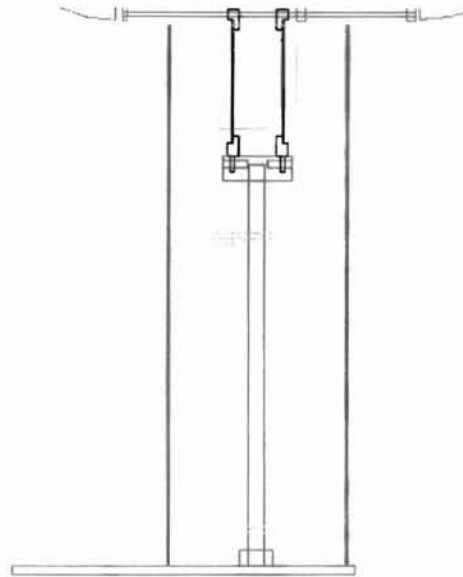


Figure 3.13 Sketch of Main Support System

This 'super-structure' is constructed from three Plexiglas forms held in place by two steel all-thread rods (Figure 3.14). The shape of the forms is to aid in the streamlining of the support, but also provides a support of the cable interfaces. The middle support is where the interface between the sensors above and the electronic systems below occurs. On this level three 15-pin D-Subminiature connectors are attached this is the point where the mechanical and electric components of the sensors interface (Figure 3.15).

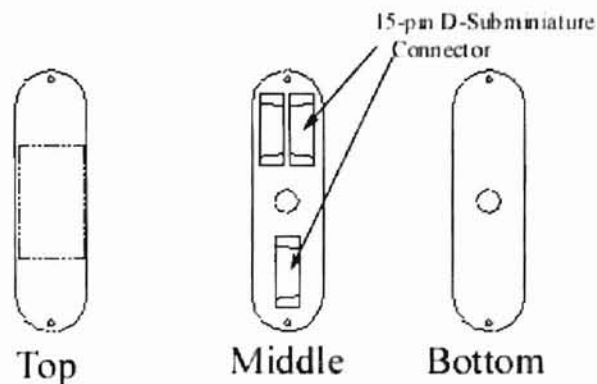


Figure 3.14 Support Forms

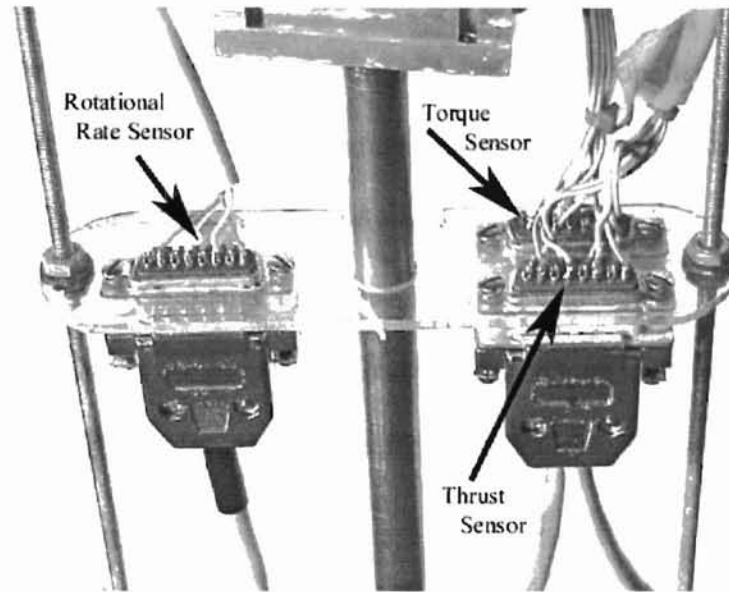


Figure 3.15 Quick Connection Points

3.3.5 Shroud

To reduce the effect of the dynamometer and support on the flow of air, a shroud was placed over the entire structure, it also protected the sensors of the dynamometer from the disturbance of air that passes around the device. The shroud itself was constructed from a foam core that was formed into the desired shape and was covered in fiber-glass and cured. After curing the foam core was removed leaving just the outer fiber-glass shell. This shell is then cut into two pieces at the point of the middle support. The lower section is attached directly to super structure with out any modification. The upper section, however has a small hatch cut out. This hatch is centered on the upper section and allows for access to the power connect interface of the motor with out removal of the shroud.

3.4 Electronic Components

To measure the force and moments produced by a propeller, it is necessary to change the strain produced in the legs of the dynamometer into a measurable quantity. To do this strain gages are used, the strain is found by a change in resistance of the gages. This change was caused by a change in the length of the gage caused by the load induced by the force and moment of the propeller. However this change in resistance is very small and one must find a way to determine this change in resistance. This was done by use of a Wheatstone bridge.

The Wheatstone bridge is composed of four legs, with one strain gage on each leg. The gages are of type CEA-13-240UZ-120 and are arranged as such to all full temperature compensation. In order to set the null point on the bridge two 10 ohm, 20 turn potentiometers are placed in two of the legs. This arrangement is shown Figure 3.16,

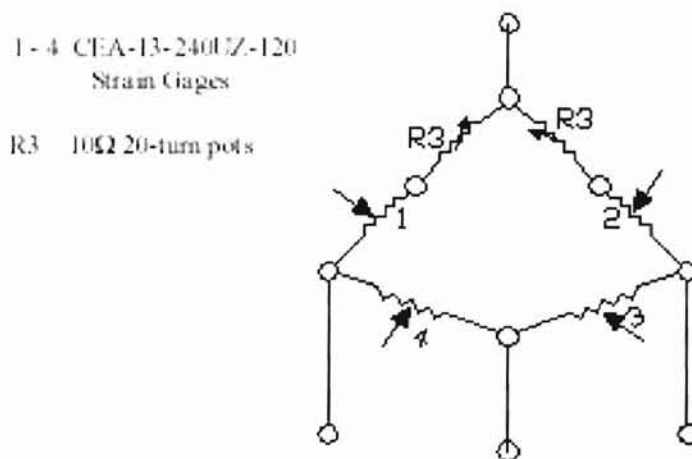


Figure 3.16 Circuit Diagram of Wheatstone Bridge

will produce an output voltage if it is not in balance. The voltage will then have to be amplified in order to be measurable, the voltage was amplified 100 times, using a two part circuit. The first part of the circuit is a signal buffer and the second was a simple non-inverting op-amp circuit. The buffer was used since both the thrust and torque were recorded on separate sub-circuits but powered by the same power supply. One of the more difficult items with this circuit setup was that the Wheatstone bridge's power supply could not be grounded, so the power to the circuit was provided by a high and low voltage source. The electrical schematic for this sub-circuit can be seen in Figure 3.17.

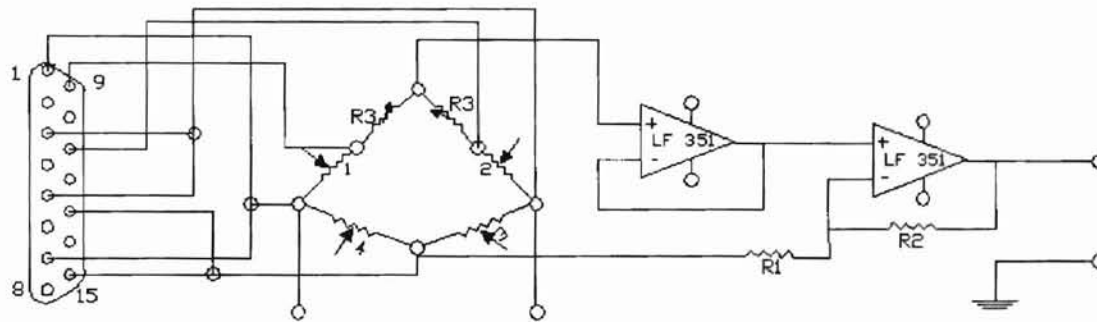


Figure 3.17 Torque/Thrust Sub-Circuit Diagram

The only other sub-circuit inside this arrangement was used to condition the signal that was produced by the rotational rate of the system. As stated earlier the rotational rate sensor consisted of an infrared emitter and detector pair. This signal if not conditioned would be hard to interpret an accurate frequency so to aid in this the signal was set through a comparator. The comparator works by looking at the signal and then only allows a fixed voltage to pass through the circuit if the reference voltage has been exceeded by the incoming voltage signal. The result of this circuit is that it transforms the incoming voltage signal into a step voltage of TTL format. This output is then easier to

be analyzed and determine the frequency of the signal. The electrical schematic for this sub-circuit can be seen in Figure 3.18

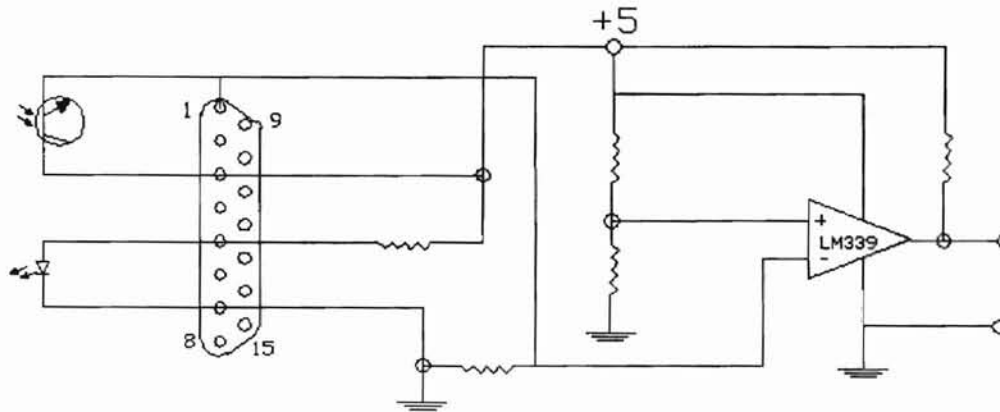


Figure 3.18 Rotational Rate Sub-Circuit Diagram

This signal is then analyzed on the oscilloscope to determine the frequency of the signal. This frequency is directly related to the rotational rate of the propeller in revolutions per second.

To aid in the 'debugging' of the electrical system, both of the Wheatstone bridge circuits are built so that they are interchangeable. The interchangeability is included in the entire design from the cables all the way to the circuit boards. The degree to which the system is interchangeable can be seen in Figure 3.19. This degree of interchangeability allows the user to quickly determine the location of any error or breakage in the system.

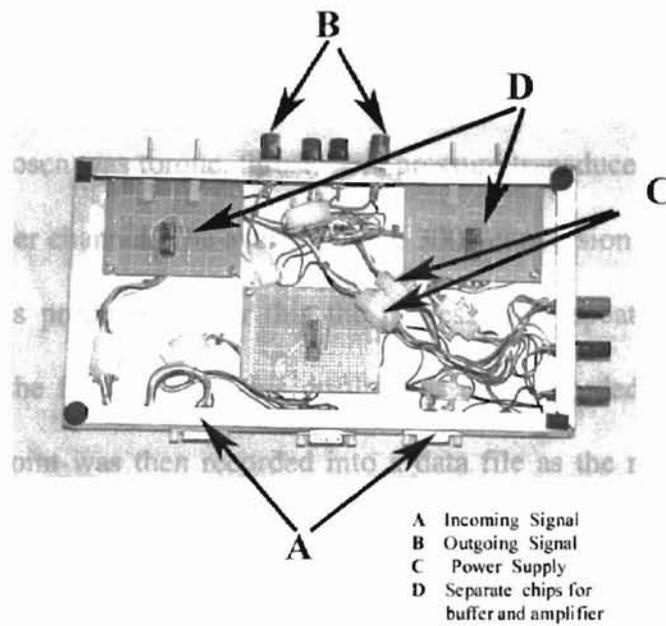


Figure 3.19 Interchangeability of Electric System

The interchangeability of the system was decided on so that it would be much easier to determine the section of the system that is not operating correctly and thus will allow the system to be repaired more quickly. The major parts of the system that are interchangeable are those that involve the thrust and torque sensors. The interchangeability starts with the cables and then proceeds all the way through the electrical system to the point at which it interfaces with the computer. Inside the electric systems box, all major components have been designed with quick change plugs. This break down of the system into five smaller components for each sub-circuit and allows one to determine the exact location of most any problem with in the systems box.

3.5 Data Acquisition

The voltage signals from the torque, thrust, pressure sensors are read and processed by a Metrabyte DAS-16 A/D board inside a 386 PC DOS based computer. For

the studies presented in this thesis, three channels were read by the computer sequentially with use of a custom written program, the source code can be found in appendix A. The order of the channels chosen was torque, thrust, and pressure transducer. The A/D board made 3000 conversion per channel. The average of the 3000 conversion is then computed and a single packet was produced. After this the process was repeated fifty times to produce an average of the fifty packets, this results was then recorded as a single data point result. The data point was then recorded into a data file as the raw voltage to be processed at a later time.

In order to determine the rotational rate of the propeller shaft the signal that was produced by its system was analyzed on an oscilloscope. The oscilloscope was setup so that it would display the frequency of the incoming signal on the screen. This results was then entered into the computer program. After this data was entered by the user, the computer would then start the data acquisition of the three channels. After the data for the three channels had been processed and recorded the user was prompted for the power that was placed into the motor. The power that was placed into the motor was found by use of an Astro Flight 'Whatt' meter, that has been placed in line between the power supply for the motor and the speed controller. This meter allows two major things, first it allows the user to maintain a power level that is below the maximum power rating of the motor. Secondly, it also can be used in order to aid the designer in determining the 'overall system efficiency'

4 EXPERIMENTAL PROCEDURE

4.1 Rational for Experimental Approach

The primary goal of this experimental investigation was to determine the dynamic performance of a range of propellers, as it was found that there was a severe lack of information available in propellers below 1 meter in diameter. This experimental investigation was accomplished by studying the resulting forces produced by the propeller at a fixed rotational rate while varying the tunnel velocities. Varying the tunnel speed allows one to determine the dynamic performance of the propeller by changing the advanced ratio. While one can also vary the rotational rate at a fixed tunnel velocity to also determine the dynamic range, this would result in a large change in the Reynolds number during the investigation. Therefore a part of this experimental investigation, was to determine the sensitivity to Reynolds number on the dynamic performance of the propeller. This was done by varying the rotational rate over a range of tunnel velocities and then comparing the results as a function of advance ratio.

In order to determine the dynamic performance result of the propeller during a run, the following are measured; thrust, torque, rotational rate and tunnel velocity. The tunnel velocity was determined with the existing equipment available in the wind tunnel facility, while the remaining three are found by use of custom built sensors. The sensors were built so as to maximize the mechanical sensitivity to minimize the need for amplification of the resulting signal.

4.2 List of Experiments Conducted

The experiments in the investigation were conducted using 10" diameter propellers inside the low speed wind tunnel facility from static to a tunnel pressure of one inch of water.

- 1) Pitch sweep with a fixed 10" diameter ($P/D = 0.3, 0.5, 0.6, 0.7, 0.8, 0.9, 1.0$)
- 2) Reynolds number effect by varying rotational rate (3600, 4800, and 7200 RPM)
- 3) Differing manufactures brand effect
- 4) Effect on tip clipping

4.3 Calibration

The very first things that must be accomplished prior to any operation of the dynamometer system is calibration. This calibration involves taking measurements with known loads and then recording the resulting voltage of each subsystem so as to acquire the data and then transform the data into useful information.

4.3.1 Torque Sensor

The procedure for the calibration of the torque sensor is as follows. A simple load beam was mounted on the centerline of the shaft and secured in place. Then by placing known weights at known locations along the beam, a measurement of the resulting moment was found. To aid in this calibration, multiple weight and distance combinations that produced the same moments were recorded during calibration. Both clockwise as well as counter-clock wise reading were taken and recorded.

Once the measurements of the voltage differences for each load was recorded, it was possible to determine the calibration curve for the torque sensor. The calibration curve was found by means of fitting the recorded data to a linear curve fit. The results of this fit are shown in Figure 4.1 and are later used to transform voltage readings into

torque measurements. The resulting error from this curve fit was found to be no more than 2.66% error.

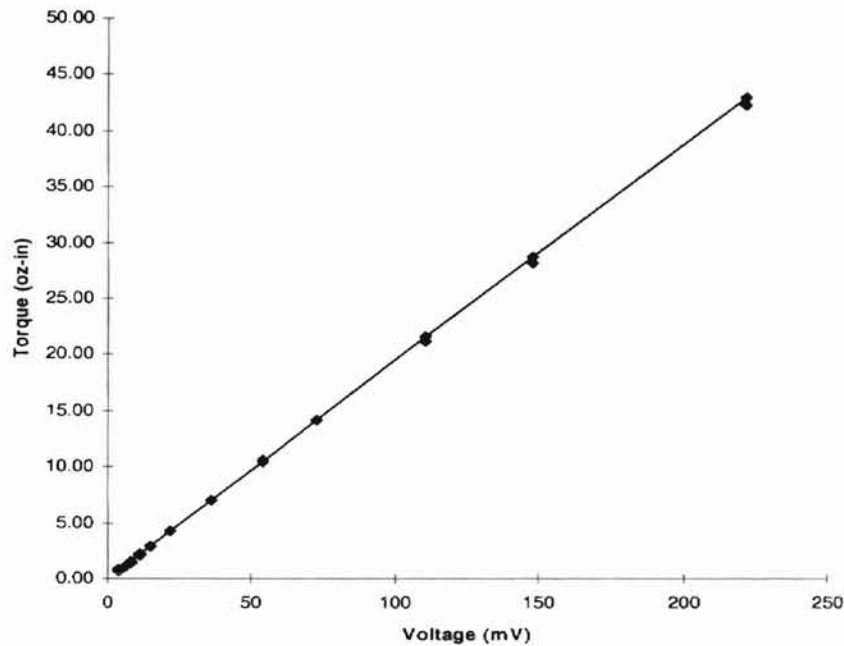


Figure 4.1 Calibration Curve of Torque Sensor

One of the final parts of calibration is to determine the tare torque.

The tare torque is defined as the torque produced by the motor when no propeller is mounted on the motor shaft. The tare torque was recorded as a function of the rotational rate of the propeller shaft. The results from this are then used to correct the torque measurements found during an actual data run.

4.3.2 Thrust Sensor

The procedure for the calibration of the thrust sensor is similar to that of the torque sensor as it really only differs in the method of the applied load; the method used to calibrate the thrust sensor is as follows. A dead weight is attached to the propeller shaft

by means of a simple pulley arrangement to calibrate for thrust, and is then attached to the rear of the system for drag.

This arrangement is used along with varying known weights in order to calibrate the thrust sensor in both the positive (thrust) and negative (drag) direction. The voltage measurement for each load was recorded, and it was then possible to determine a calibration curve for the thrust sensor. The calibration curve was found by means of fitting the recorded data to a linear curve fit. The results of this fit are shown in Figure 4.2 and are used to transform voltage readings into thrust measurements. The error from this curve fit resulted in no more than 2.04% error from the actually result.

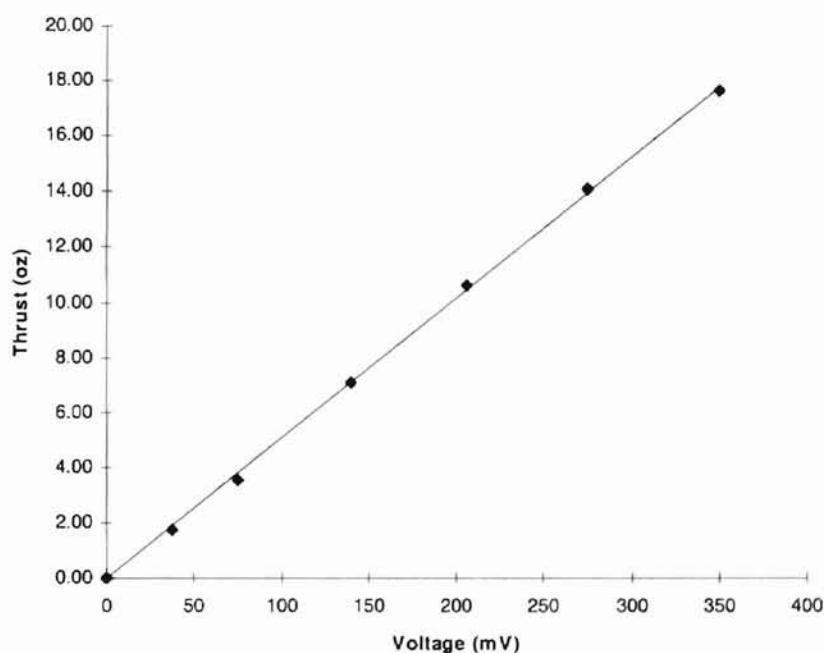


Figure 4.2 Calibration Curve of Thrust Sensor

The next item that had to be determined for the thrust sensor was the tare drag on the system at differing tunnel velocities, it should be noted that this is the tare drag only on the dynamometer system and as such no propeller should be mounted. This section of

the calibration must be done so the actual thrust that is produced by a propeller can be determined and the effects of drag caused by the dynamometer can be removed. It is for this reason that the calibration of the system included both positive and negative loadings. The results of the tare reading are shown in Figure 4.3. From this data a second order curve fit was used in order to determine an equation to be used later in the data analysis and results in an error of 1.00% to the calculated tare drag.

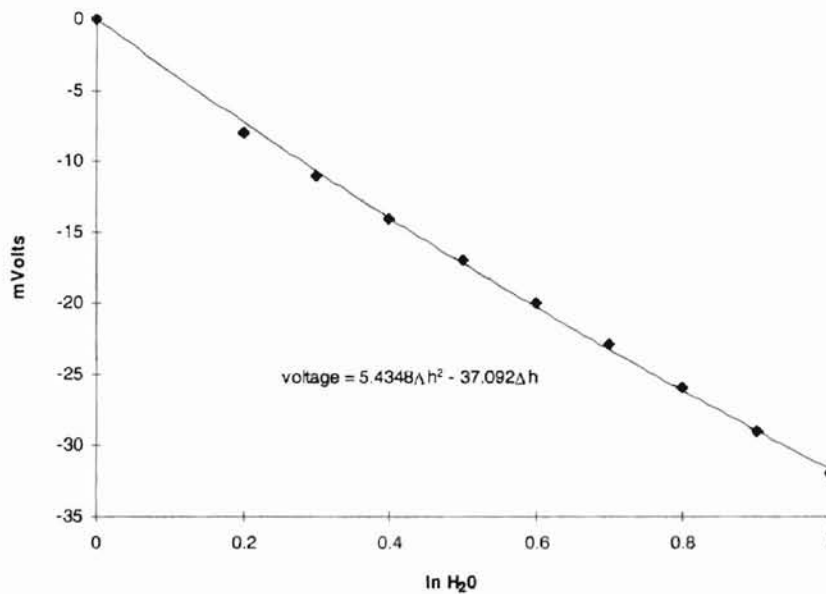


Figure 4.3 Tare Drag of Dynamometer

4.3.3 Rotational Rate

Since the rotational measurement already produced a signal that could be measured as a frequency, the rotational rate of the propeller shaft could be found directly without any need for calibration. However to confirm this, a calibrated strobe light was used to verify that the indicated rotational rate was the correct rate. To determine the rotational rate of the propeller and thus the propeller shaft, a mark was made on only one

blade of the propeller. The mark on the blade was then tracked with by use of the strobe light. It was found that the reading indicated on the calibrated strobe light matched that of the rotational sensor. Since the two reading appear to match, it can be assumed that the rotational rate indicated by the system is within the precision of the stroboscope as published by the manufacture, 0.01% of the LSD.

4.4 Data Acquisition and Processing

Once the calibration for the sensors has been found, the data that is recorded can be mapped into corresponding units. To aid in the recording a small program by the name of 'SETUP.EXE' was written and is used to determine the current settings of the sensors provides the needed range for a given propeller being tested. After confirmation of the range with this program, the main custom written data acquisition program , 'PROPSCAN.EXE', is started.

After the main program 'PROPSCAN.EXE' is started, the user is prompted for the upper and lower channels to be scanned. It is important to note at this time that the sensors are designed to be recorded in the following order; torque, thrust, and tunnel pressure. The next items that the user is prompted for are the current corrected atmospheric pressure and the current tunnel temperature. This information is used to determine the current properties of the air.

The current atmospheric pressure is found by use a barometer that is located in the wind tunnel facility and the tunnel temperature is found by use of a thermocouple that has been mounted inside the test section. Next the user is prompted for the name of the data file to be recorded, it should be noted here that the name of the file is limited to only eight

characters. After this the user is prompted for the number of packets that they would like to be recorded.

Each packet of data contains the of average 3000 samples from a single channel. The packets themselves are then again averaged to produce a single piece of data. The data recording is started after the user enters the current rotational rate of the propeller shaft. After the user enters this information the computer then records and stores this data point, as soon as the computer has processed and stored the data the user is then prompted to enter the current power setting for the motor.

The program then returns to a standby setting until the user enters a new rotational rate at which time the program then repeats the process over. In order to end the program the user needs to enter a negative number for the rotational rate. After the program has ended the data file that has been created is now ready to be processed. The data is processed into usefully information by use of an Excel spreadsheet.

The data is imported into a spreadsheet where it is processed. The spreadsheet processes the raw voltages that were recorded by the computer into 'engineering units' so that the coefficients can be found. The data that is imported in to the spreadsheet is as follows; corrected barometer reading, tunnel air temperature, dynamic viscosity, density of air, velocity conversion and then in tabular format tunnel velocity, rotational rate, thrust, torque, power input. A sample of the data that is imported is shown below in Table

4.1

Corrected Barometer Reading (mm Hg)	746.5			
Tunnel Air Temp (c)	31.5			
Dynamic Viscosity (lbm/ft-s)	1.26E-05			
Density of Air (lbm/ft^3)	0.07106			
Vel Conversion (ft/sec /sqrt(in H2))	68.5676			
Tunnel Velocity (ft/sec)	RPS (Rev/Sec)	Thrust (mV)	Torque (mV)	Power Input (Watts)
0	0	-279	8	0
16.8	120	-23	-43	125
16.37	80.65	-191	-13	52
16.37	60.24	-248	-3	30

Table 4.1 Sample of Imported Raw Data

Once the data has been imported it is processed and the following are calculated; tunnel pressure, rotational velocity, propellers wind velocity, Reynolds number, tare drag, actual thrust, thrust/drag in ounces, torque in ounce-inches, advance ratio, and then the coefficients of thrust, torque, and power. Followed by the propeller efficiency, then finally the ratio of the thrust and power coefficients. After all the given data for an experimental investigation has been processed it is then sorted first by the rotational rate and then advance ratio.

4.5 System Repeatability

This dynamometer system would not be very useful if it did not provide both repeatable and accurate results. In order to determine the repeatability of results from this system numerous identical runs were performed on differing days. The identical runs were composed of the following; multiply rotational rates, variable tunnel velocities, and several propellers of the same pitch, diameter and brand. The results of the repeatability

test indicated that the coefficients of torque and thrust varied by less than 1.62% and 1.13%, respectively. The results are also shown graphically in Figure 4.4 and Figure 4.5.

While the variation of the propeller efficiency was higher than that of the two coefficients, as much as 1.92%, this is to be expected since it is composed of both previous coefficients as well as the advance ratio this would be expected. The results of the propeller efficiency section of the repeatability are shown in Figure 4.6

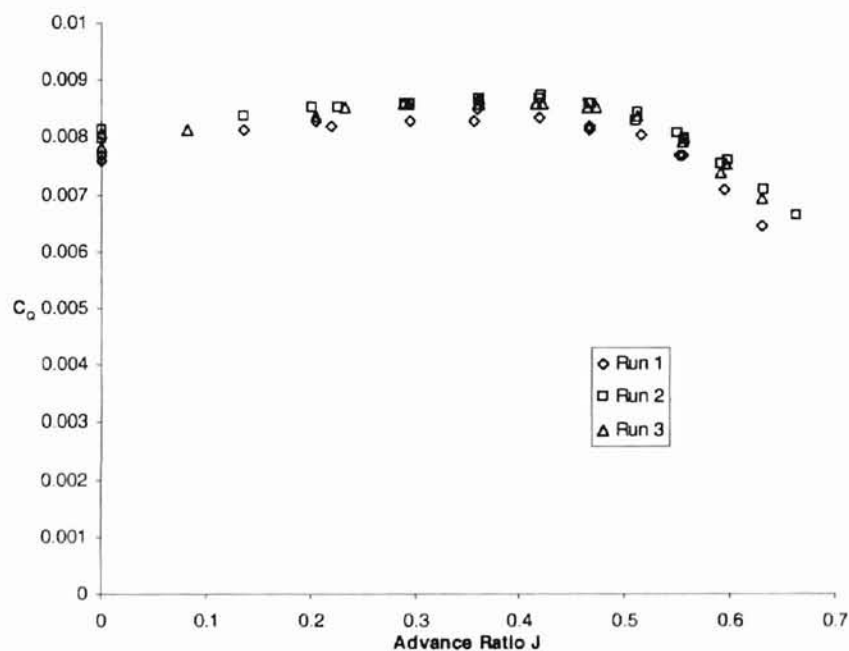


Figure 4.4 Repeatability Test of Torque Coefficient

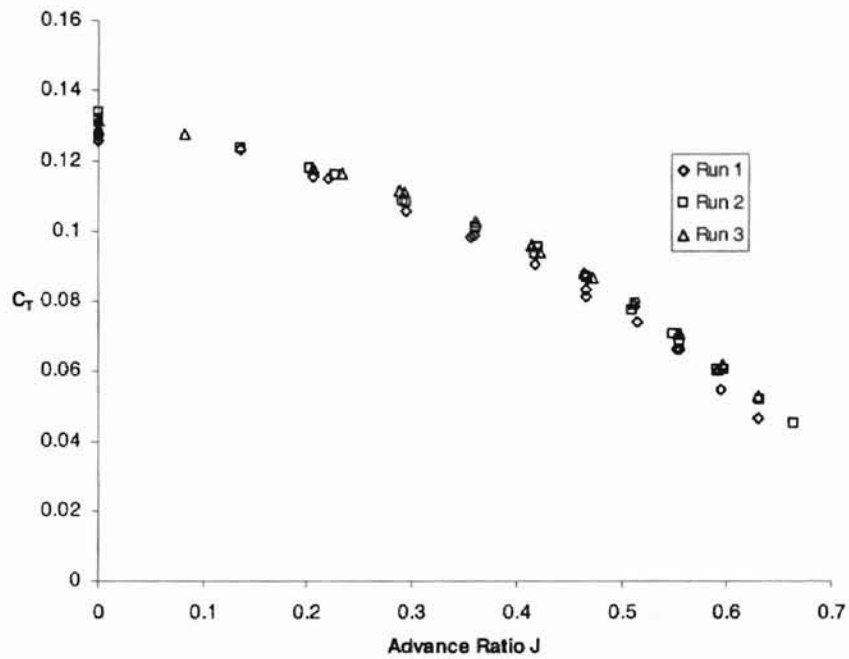


Figure 4.5 Repeatability Test of Thrust Coefficient

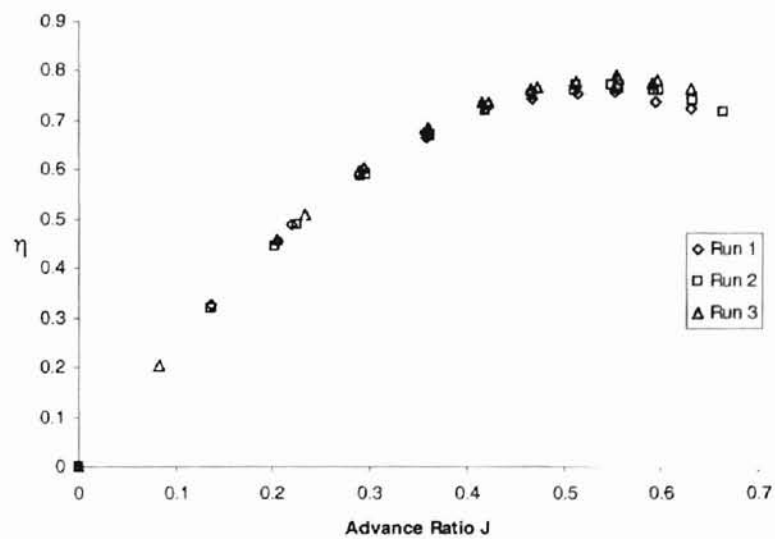


Figure 4.6 Repeatability Test of Propeller Efficiency

4.6 Signal Quality

Even with the high repeatability of the system, the quality of the signal must be analyzed. The main reason that it must be looked at is that while the results are represented as a steady state processes, this is not the case. The signal actually varies around this steady DC signal, the amount at which it varies is do to the vibration of the system at a frequency of the blade rotational rate. The amount at which it varies will be considered the noise. In order to determine the amount of 'noise' in the system a digital oscilloscope was used to analyze the time waveform of the signal for varies rotational rates. An example of the waveforms at rotational rate of 60, 80, and 100 RPS can been seen in the following six figures (Figure 4.7 - Figure 4.12).



Figure 4.7 Waveform of the Thrust Signal at 3600 RPM

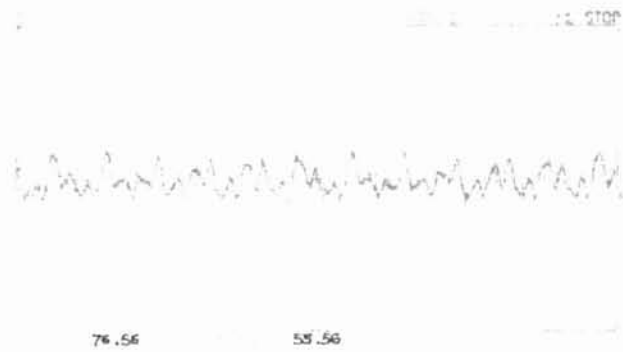


Figure 4.8 Waveform of the Torque Signal at 3600 RPM



Figure 4.9 Waveform of the Thrust Signal at 4800 RPM

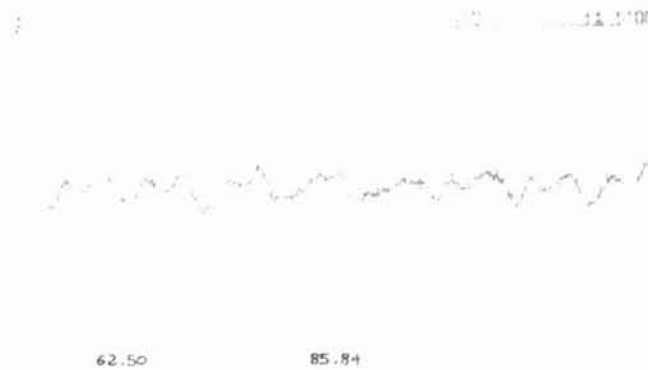


Figure 4.10 Waveform of the Torque Signal at 4800 RPM

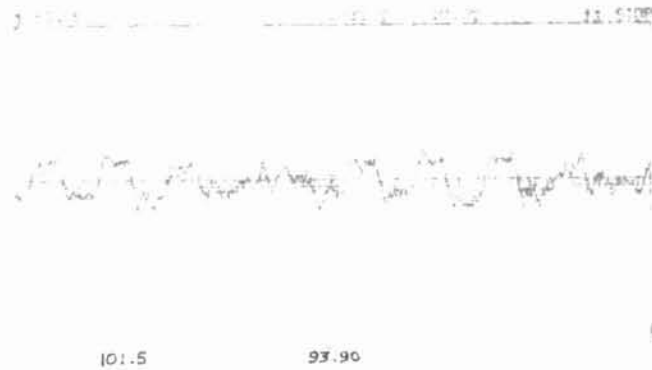


Figure 4.11 Waveform of the Thrust Signal at 6000 RPM



Figure 4.12 Waveform of the Torque Signal at 6000 RPM

With the use of the oscilloscope the peak to peak voltage as well as the voltage rms was recorded for several runs, the results were then averaged in order to determine the average 'noise' (peak to peak) and average DC signal (voltage rms). After this a signal to noise ratio was found with use of:

$$\frac{S}{N} = \left(\frac{v_s}{v_n} \right)^2 \quad (4.1)$$

With use of this equation the signal to noise ratio over the range of 3600 to 7200 RPM in steps 600 RPM. The results of this indicate that one must carefully select the

rotational rate of the investigation in order to avoid areas which contain low signal to noise ratios.

Unfortunately as can be seen in Figure 4.13 and Figure 4.14 the worst case for the signal to noise ratio does not overlap for both channels simultaneously. The signal to noise ratio on the thrust channel appears to increase with as the rotational rate increases, however this ratio does appear to peak at 6600 RPM. Where as the torque channels appears to increase until the rotational rate of 5400 RPM is reached, this appears to be the lowest ratio. However, the ratio does appear to then rapidly increase after this rotational rate.

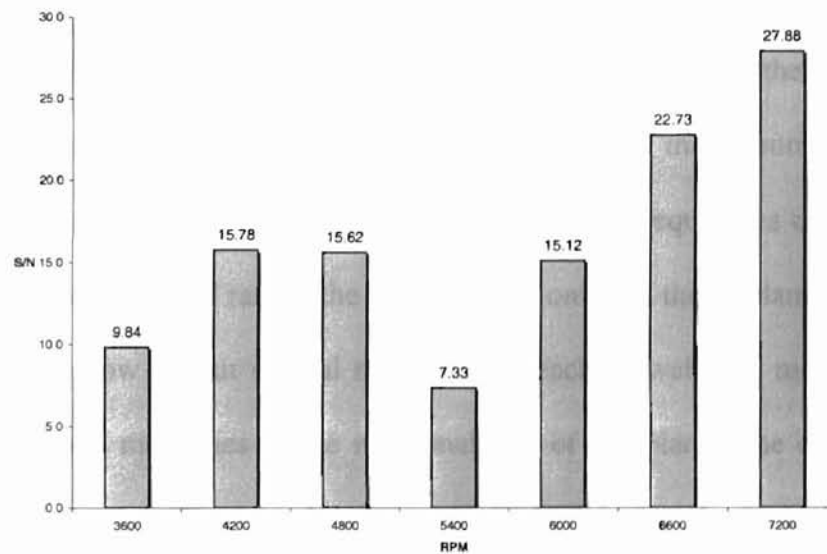


Figure 4.13 Signal to Noise Ratios for Torque

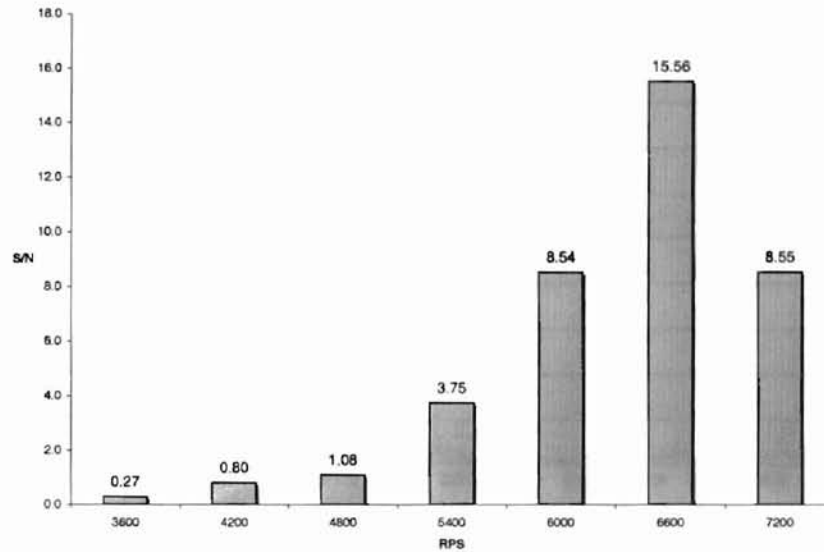


Figure 4.14 Signal to Noise Ratios for Thrust

In order to determine the nature of the 'noise' a spectrum analyzer was used in order to perform an FFT on the signal. The results of this show that the main source of 'noise' in this system comes from several know sources. The main sources of this noise are as follows; the rotational rate of the blades, the natural frequencies of the thrust and torque sensors, the rotational rate of the gearbox. Not only did the fundamental frequency of each of these show up but several multiplies of each as well, the most dominate of these being the odd multiplies of the rotational rate of the blade. The one other major item of interest that was discovered with use of the FFT is that the 'noise' is dominated by only frequencies below 500Hz and that any frequency above this point did not appear to contribute significantly to the 'noise' level. The results of three rotational rates are shown in the following figures (Figure 4.15 thru Figure 4.20).

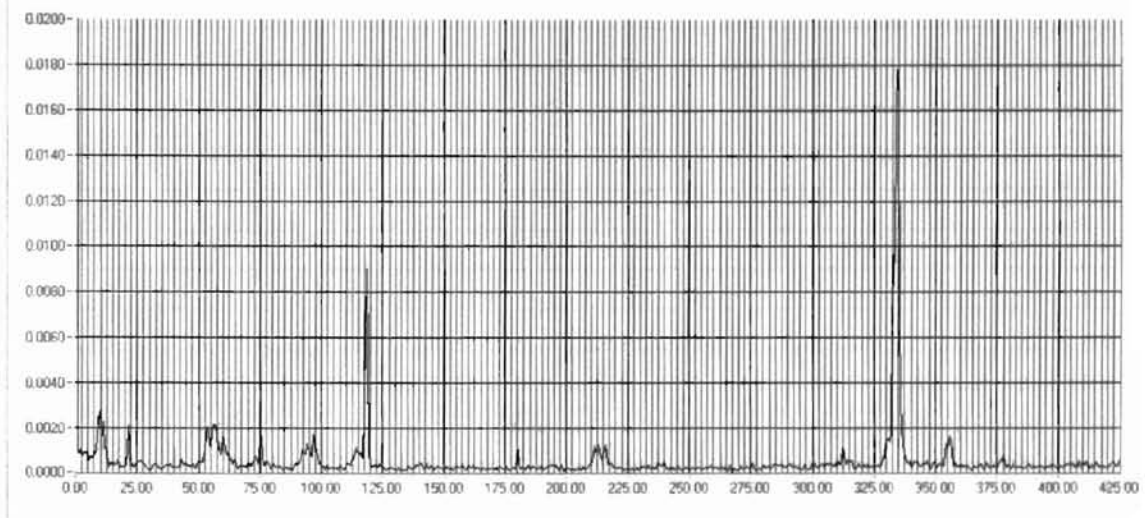


Figure 4.15 FFT for Thrust at 120 RPS

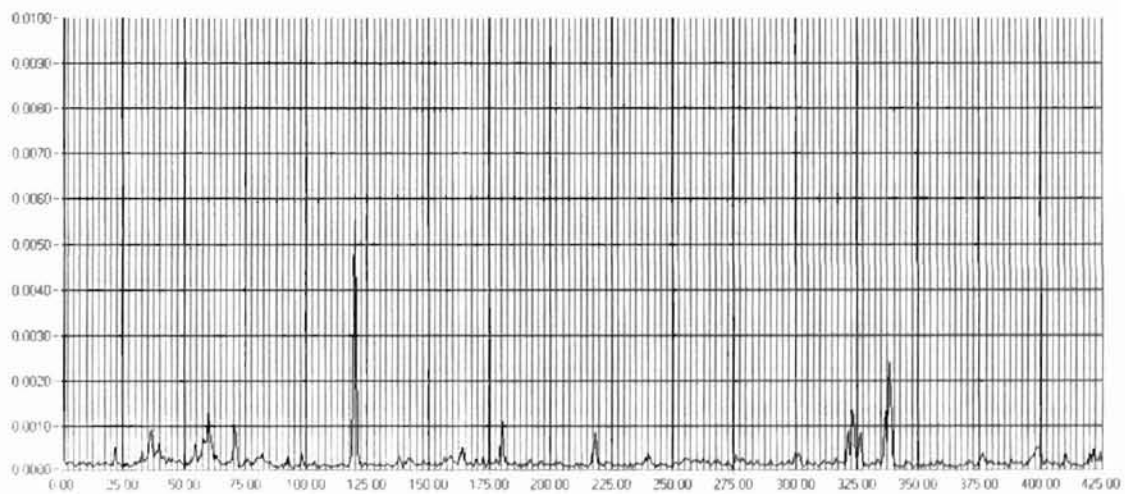


Figure 4.16 FFT for Torque at 120 RPS

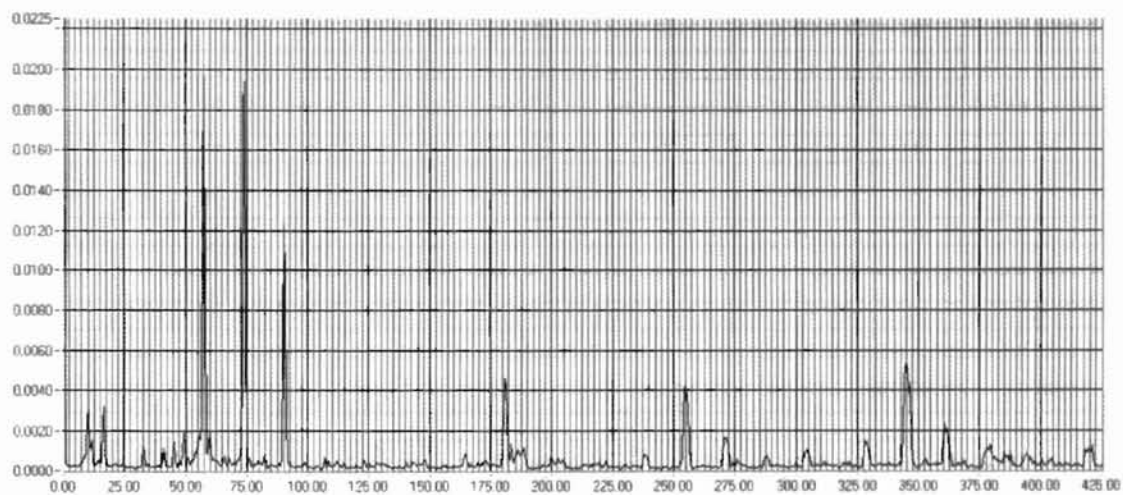


Figure 4.17 FFT for Thrust at 90 RPS

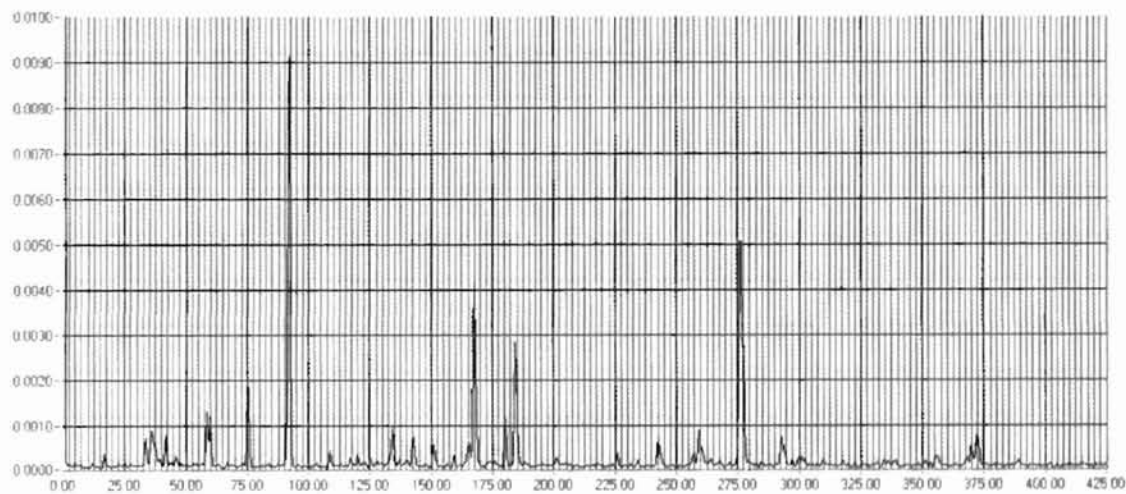


Figure 4.18 FFT for Torque at 90 RPS

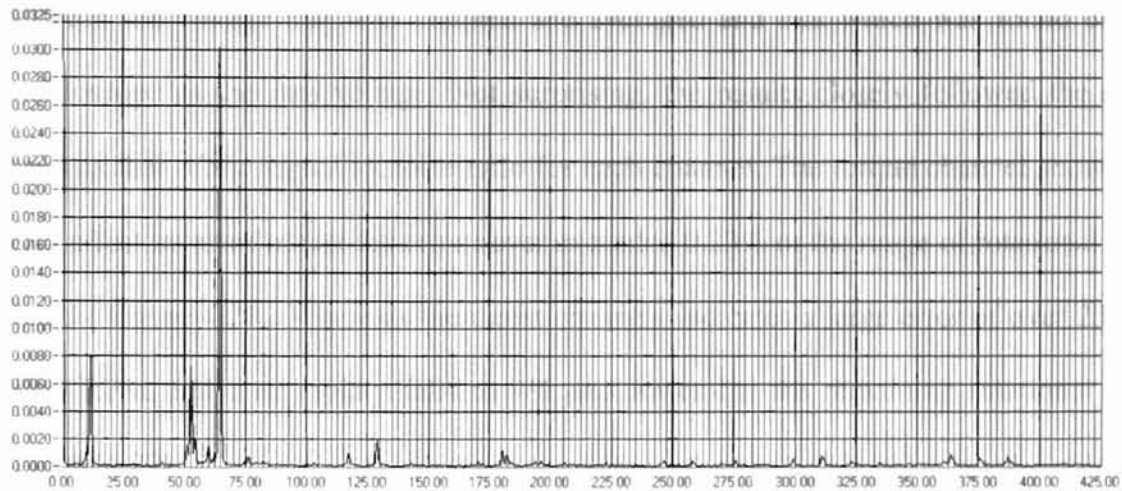


Figure 4.19 FFT for Thrust at 60 RPS

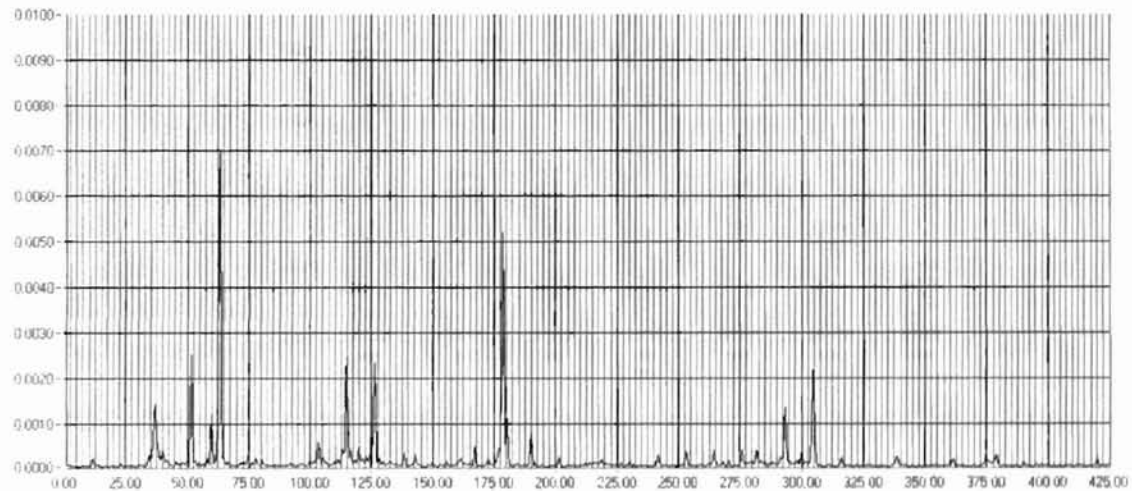


Figure 4.20 FFT for Torque at 60 RPS

With the upper frequency of interest below 500 Hz and that the 'noise' is not random in nature the selected sampling rate of 10,000 Hz proved to be more than adequate. This sampling rate along with a 15 second sample time appears to allow an accurate recording of the DC signal by means of a simple averaging of the points captured during this record length, there are 15,000 points recorded. To determine the overall effect of this sampling rate as well as the effect of the 'noise' a simple investigation was conducted in order to determine the amount of error that was observed

between the voltage that was sampled and averaged and that which was found on the oscilloscope as the rms voltage. Not surprising, the results closely followed the same trend as that of the signal to noise ratio for each channel. The torque channel shows the least effect on error in fact the error never exceeded 0.23% or the range of rotational rates tested (Figure 4.21). Where as the thrust channels indicates a large error of over 25% at 3600 RPM, but then rapidly falls to 4% and lower for the remaining rotational rates (Figure 4.22)

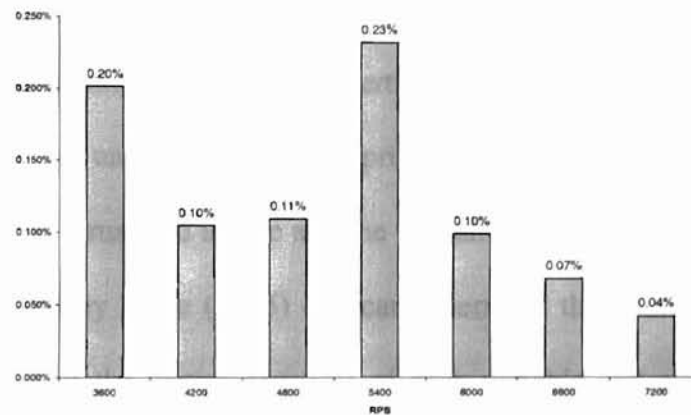


Figure 4.21 (Torque) Percent Error Between Avg. Voltage and Voltage RMS

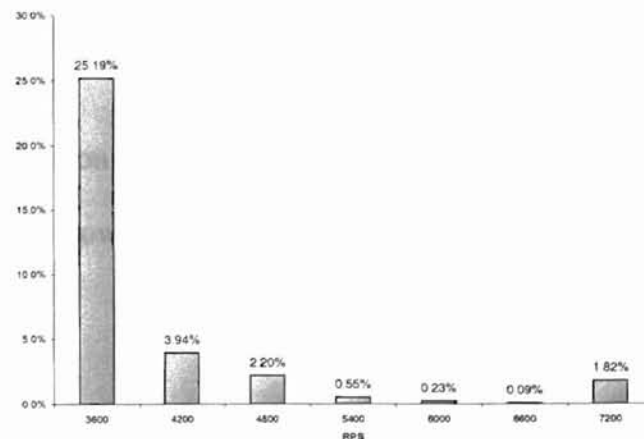


Figure 4.22 (Torque) Percent Error Between Avg. Voltage and Voltage RMS

From the results of the signal quality investigation it can be seen that this system should not be used at 60 RPS this rotational rate can produce up to 25% error on the thrust channel results, but care should also be taken at any new rotational rate that was not covered in the initial investigation it insure that not only is the signal to noise ratio high, but that the voltage found with use of the computer and A/D board closely agrees with the rms voltage that is recorded on the oscilloscope.

4.7 Uncertainty

Since one of the main goals of this investigation was to create a dynamometer that had not only high repeatability but also low uncertainty. It was decided to use the method of Kline to determine the uncertainties of the primary results of interest. These results being the coefficients of thrust and torque and the overall propeller efficiency. According to the approach outlined by Kline (1985) one can determine the overall uncertainty by finding the square root of the partial derivates of each variable and also determine the sensitivity that each separate variable has on the overall uncertainty. The equation (4.2) is the general form that is followed for each.

$$\frac{W_R}{R} = \sqrt{\left(\frac{\partial \ln R}{\partial \ln x_1} \frac{W_{x_1}}{x_1}\right)^2 + \left(\frac{\partial \ln R}{\partial \ln x_i} \frac{W_{x_i}}{x_i}\right)^2} \quad (4.2)$$

With use of this equation the uncertainty of each of the major equations used was found the results of this are shown in Table 4.2

Coefficient	% Min Error	% Avg Error	% Max Error
J	$\pm 0.179 \%$	$\pm 0.762 \%$	$\pm 3.335 \%$
C_T	$\pm 1.107 \%$	$\pm 1.110 \%$	$\pm 1.113 \%$
C_P	----	$\pm 2.040 \%$	----
η	$\pm 2.328 \%$	$\pm 2.500 \%$	$\pm 4.065 \%$

Table 4.2 Uncertainty of Major Equations

5 EXPERIMENTAL RESULTS AND DISCUSSION

5.1 Reynolds number effect

The first of investigations that was conducted was to determine the Reynolds number effect on the dynamic propeller performance. To accomplish this three different rotational rates were used, while the velocity of the tunnel was swept from static to one inch of water. By utilizing this method, the Reynolds number at a given rotational rate did not vary by more than 5%. The three rotational rate selected were 3600, 4800, and 7200 RPM and the corresponding average Reynolds numbers were 50000, 77000, and 114000.

It was observed that during this phase of the investigation that none of the coefficients or the efficiency appears to vary by more than 2.6%. The results of this can be seen in Figure 5.1 thru Figure 5.3. In order to help clarify any difference that may actually occur, a ratio between the thrust and power coefficients was developed. This ratio, which is shown in Figure 5.4, can be used by the designer in a similar fashion as the lift over drag curve. This graph will allow the designer to quickly see which propeller or blade set will produce more thrust for a given power. As any set of curves which appear above another will require less power for a given thrust setting.

It should be noted that while the effect of differing rotational rates did not appear to affect the overall performance of the propeller, it does have an effect on the static performance. However, the only coefficient that appears to be significantly affected is the thrust. The thrust coefficient increases by as much as 7% with a doubling of the

rotational rate from 3600 to 7200 RPM, where as the power coefficient changed by less than a percent for the same increase in rotational rate.

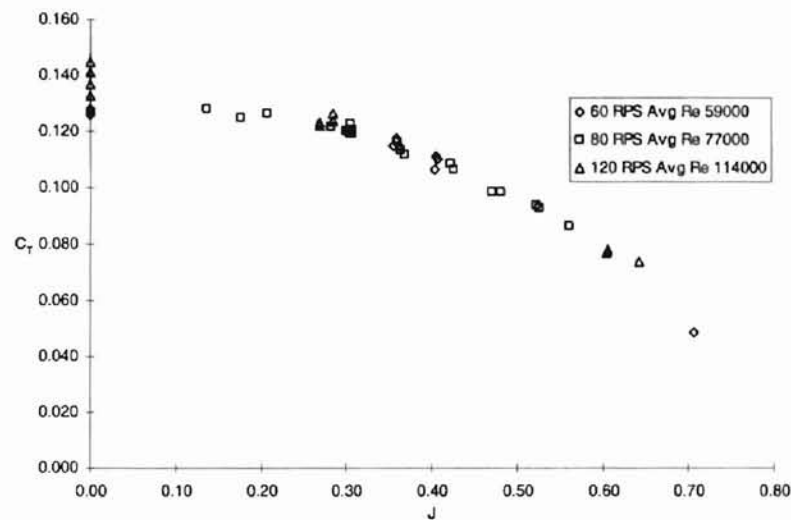


Figure 5.1 Reynolds Number Effect on Thrust Coefficient

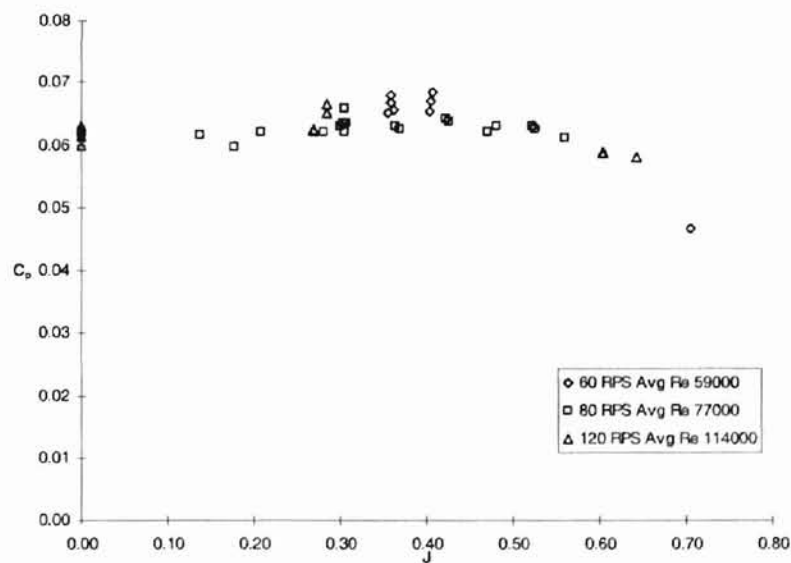


Figure 5.2 Reynolds Number Effect on Power Coefficient

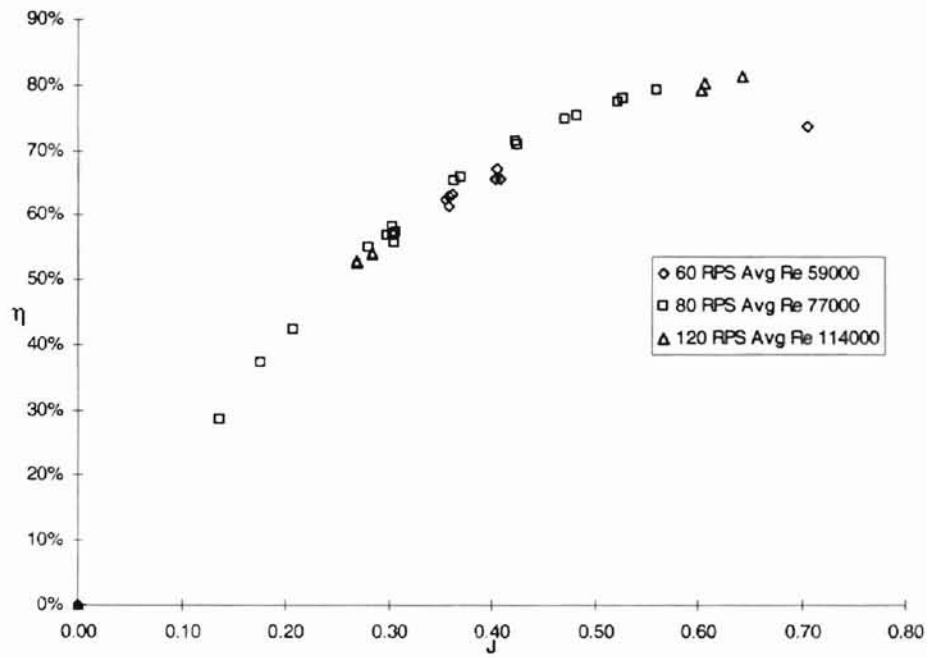


Figure 5.3 Reynolds Number Effect on Propeller Efficiency

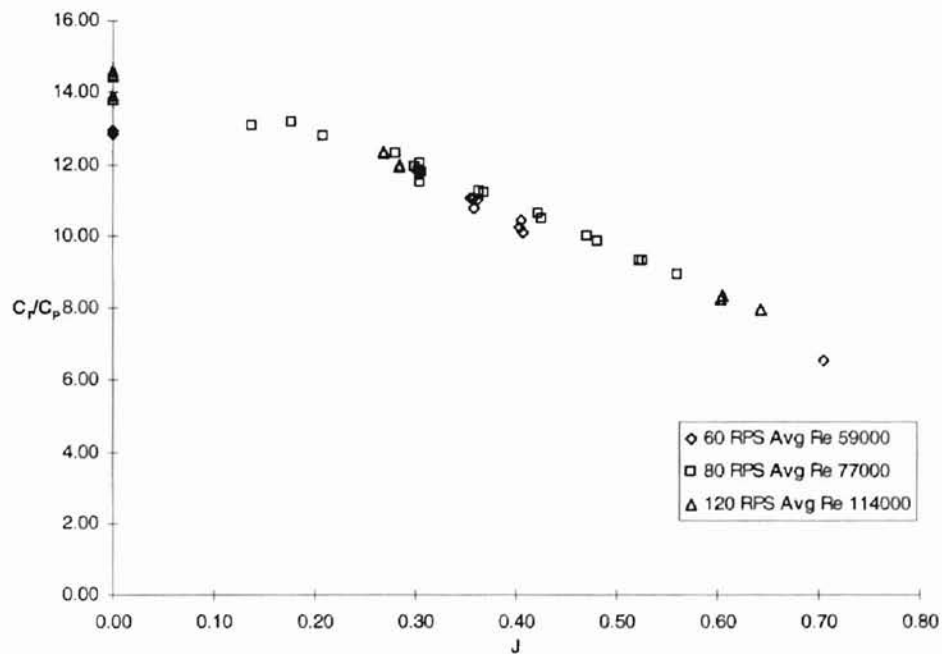


Figure 5.4 Reynolds Number Effect on the Ratio of Thrust and Power Coefficient

5.2 Pitch sweep

Now that the effect of Reynolds number had been found and it appears that it does not have a major effect on the results outside the static range, an investigation into the effect of pitch on the overall performance can now be analyzed.

In order to conduct this investigation, it was decided that only the pitch would change, as such a range of propellers all having the same diameter but varying pitches were selected. The test was conducted at a fixed rotational rate of 4800 RPM while varying the tunnel speed from static to one inch of water. The rotational rate was selected do to the power requirements of the higher pitched propeller, and in order to maintain a constant rotational rate.

It can be shown from the results that as the pitch increase the thrust coefficient increases as well (Figure 5.5), unfortunately the corresponding power coefficient increase as well (Figure 5.6). The other major item that can be seen with the increase in pitch is the advance ratio at which the propeller starts to enter the braking stage. The braking stage is encountered as the thrust coefficient approaches zero, and as expected the power coefficients lags and approached the zero axis at a higher advance ratio. The higher advance ratio was expected, as this is windmilling stage and closely follows the braking stage.

It is with use of the propeller efficiency and ratio between the thrust and power coefficients that the effect of pitch becomes the most clear (Figure 5.7 - Figure 5.8).

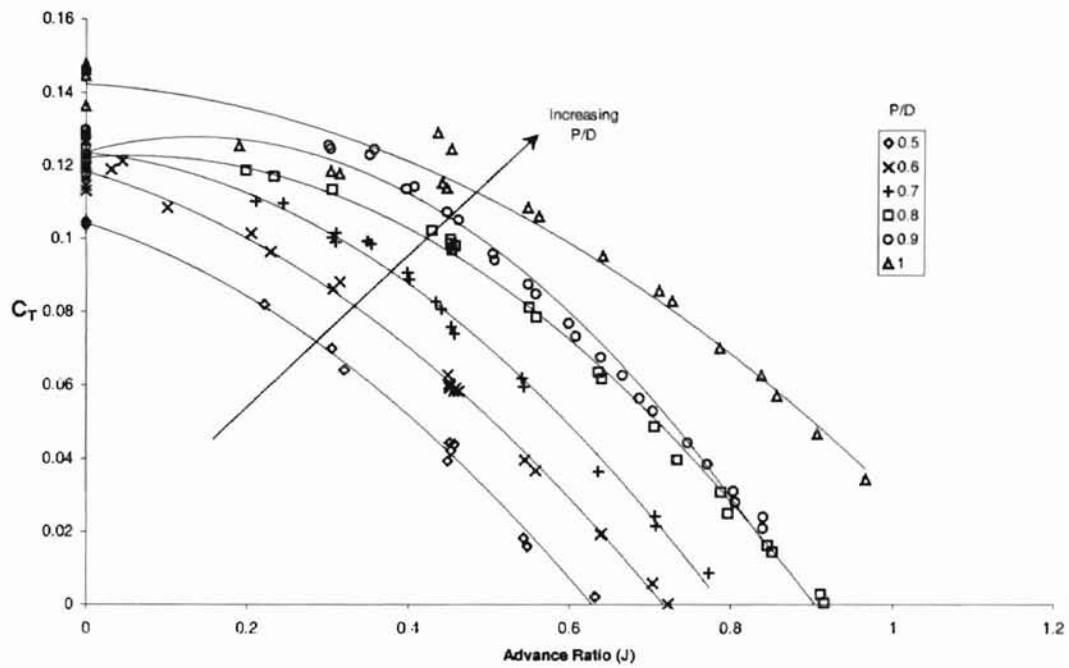


Figure 5.5 Pitch Effects Thrust Coefficient

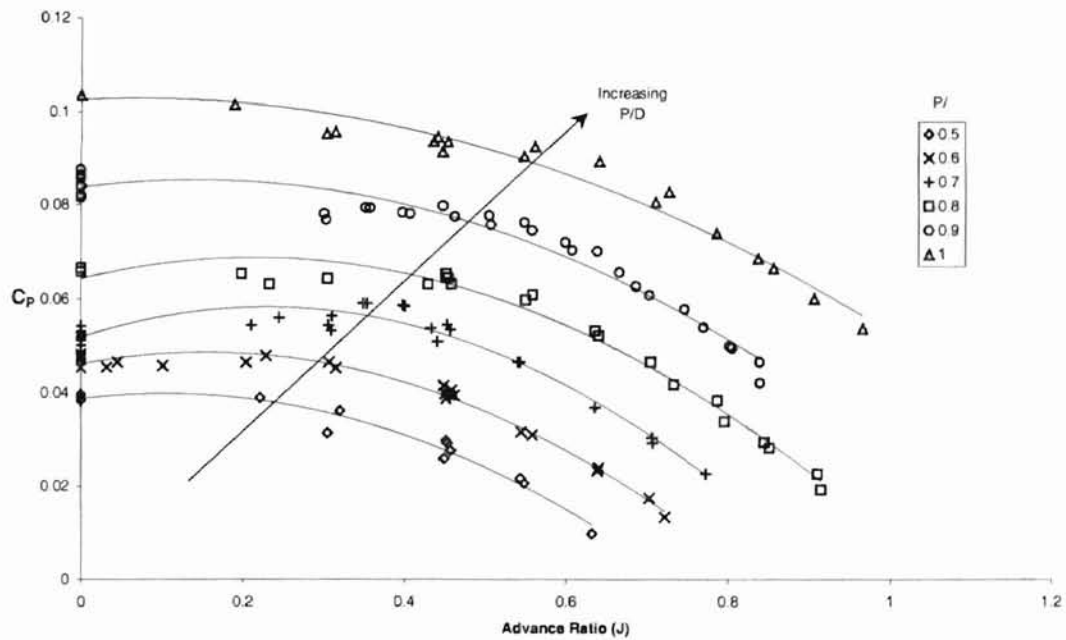


Figure 5.6 Pitch Effects on Power Coefficient

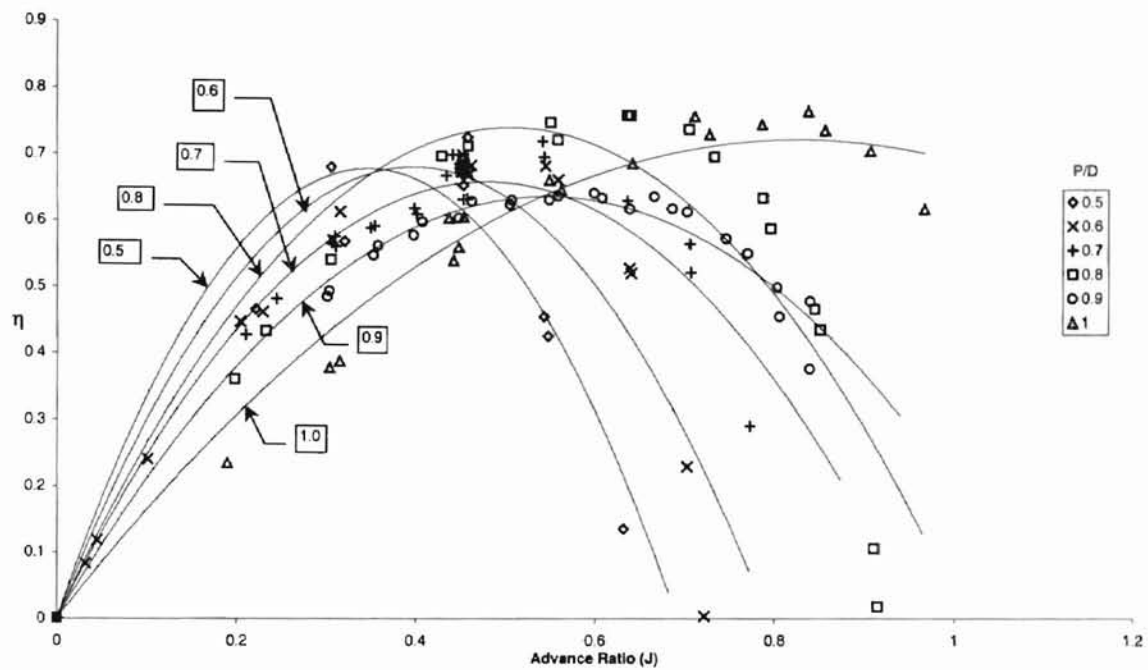


Figure 5.7 Pitch Effects on the Propeller Efficiency

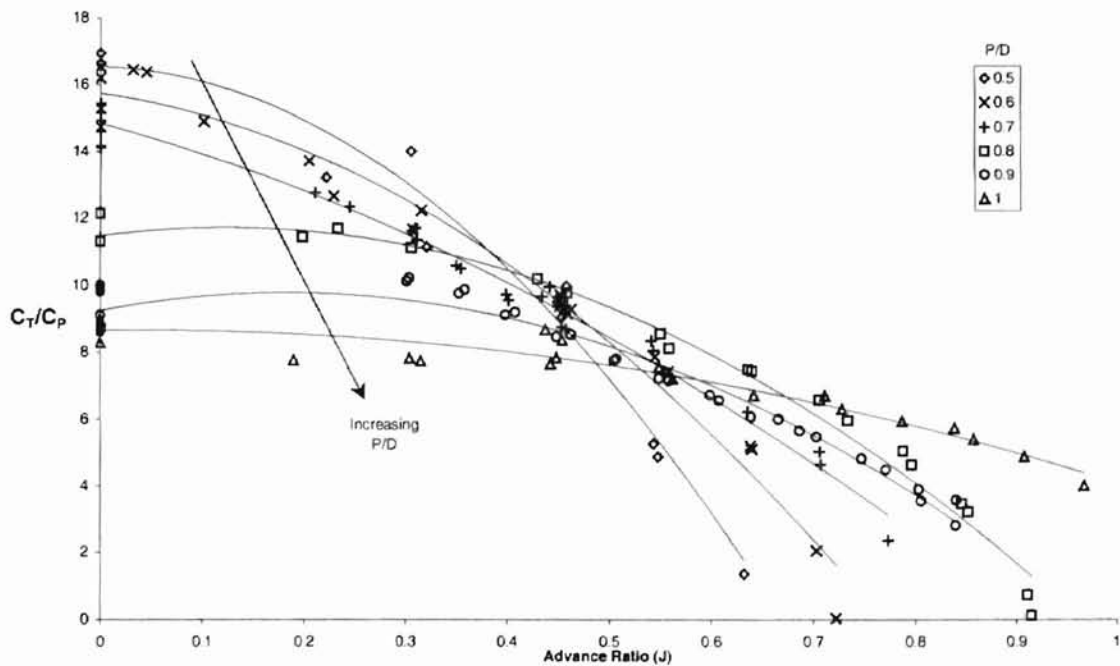


Figure 5.8 Pitch Effects on the Ratio of Thrust and Power Coefficients

5.3 Brand effect

The brand effect investigation involves analyzing the effect of the different manufacturing brand names of propellers available. In order to conduct this investigation, it was decided that only the brand of the propeller would change, while the pitch and diameter were fixed. The test was conducted at a fixed rotational rate of 7200 RPM while varying the tunnel speed from static to one inch of water.

It was observed that during this investigation that the largest increase in the coefficients appear to be between 'Brand A' and 'Brand C' and varied by as much as 30% and as much as 20% between 'Brand A' and 'Brand C'. However, at the same time the point of the braking state also increased, 'Brand A' having the largest of the three. The results of this can be seen in Figure 5.9 and Figure 5.10.

While it appears that only 'Brand A' has a dramatic increase in performance it should be noted that both coefficients increased at about the nearly the same rate, therefore the overall propeller efficiency does not increase between 'Brand A' and 'Brand C' but actually decreases. The decrease in the propeller efficiency, Figure 5.11, however is only 4.2% at most between 'Brand A' and 'Brand C', and 5% between 'Brand A' and 'Brand B'. This smaller effect on the brand can be seen most clearly in Figure 5.12. Here the results show that while at first it appeared that 'Brand A' outperformed the other two, it actually has a lower thrust to power ratio than the other two brands, but has a longer range and smaller slope than the other two brands and as such can be the better of the three brands at a higher advance ratios.

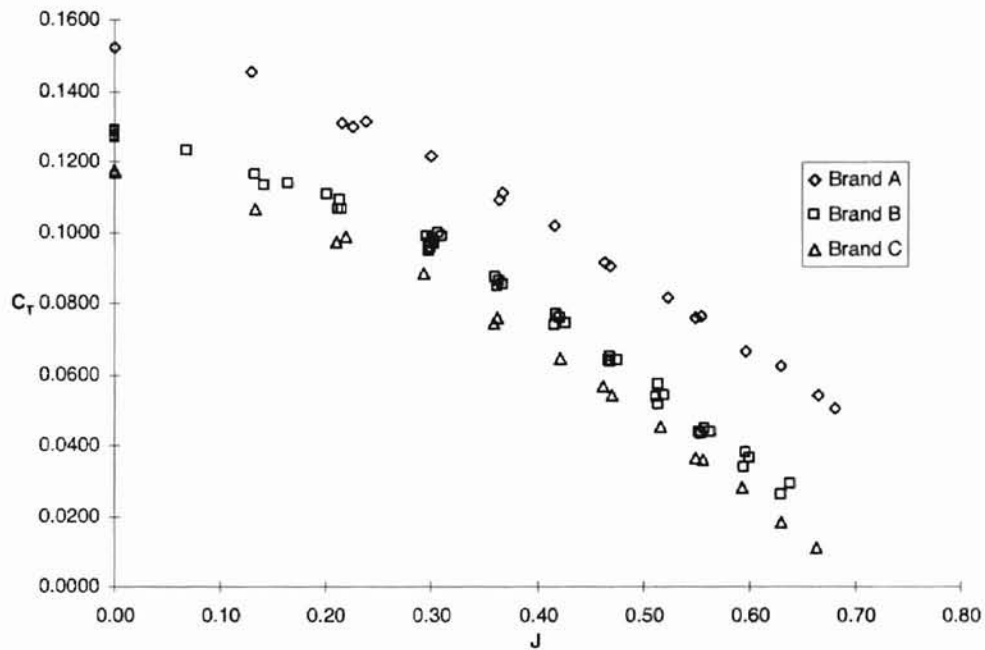


Figure 5.9 Differing Brand Effects on the Thrust Coefficient

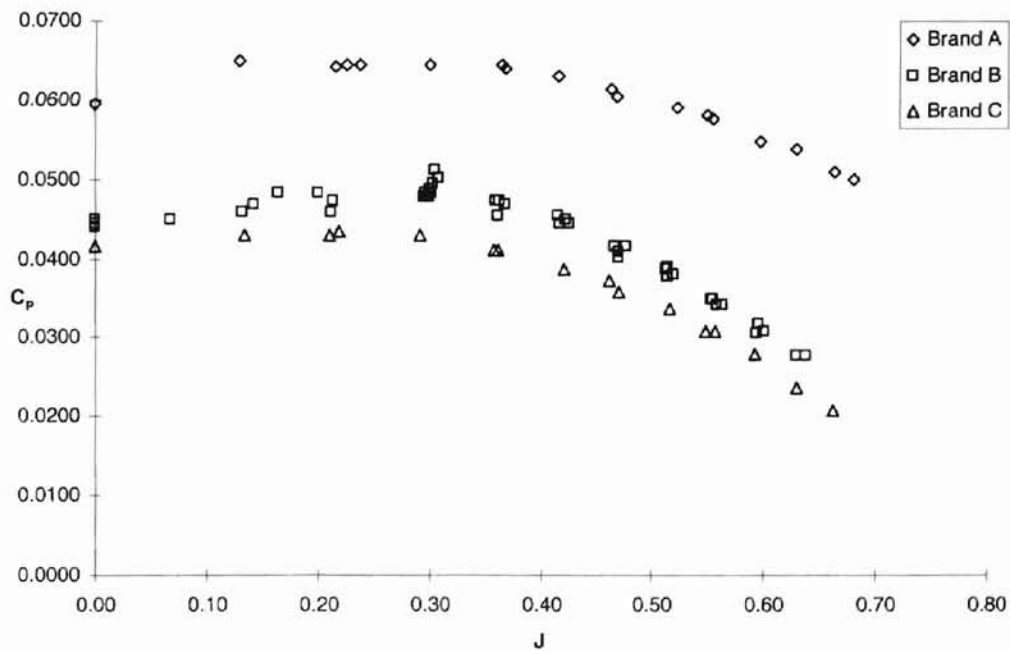


Figure 5.10 Differing Brand Effects on the Power Coefficient

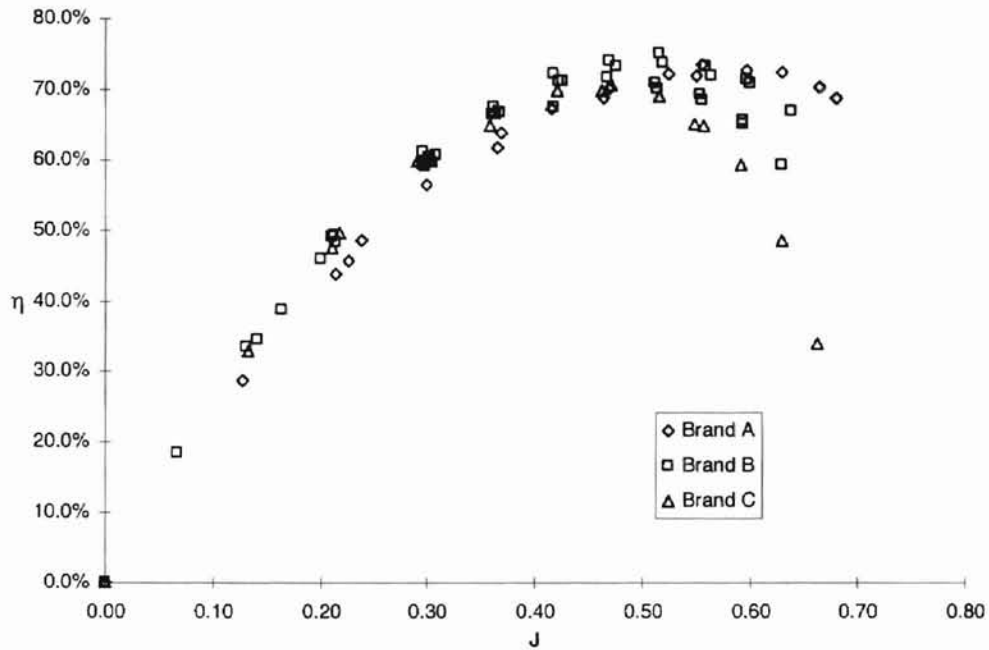


Figure 5.11 Differing Brand Effects on the Propeller Efficiency

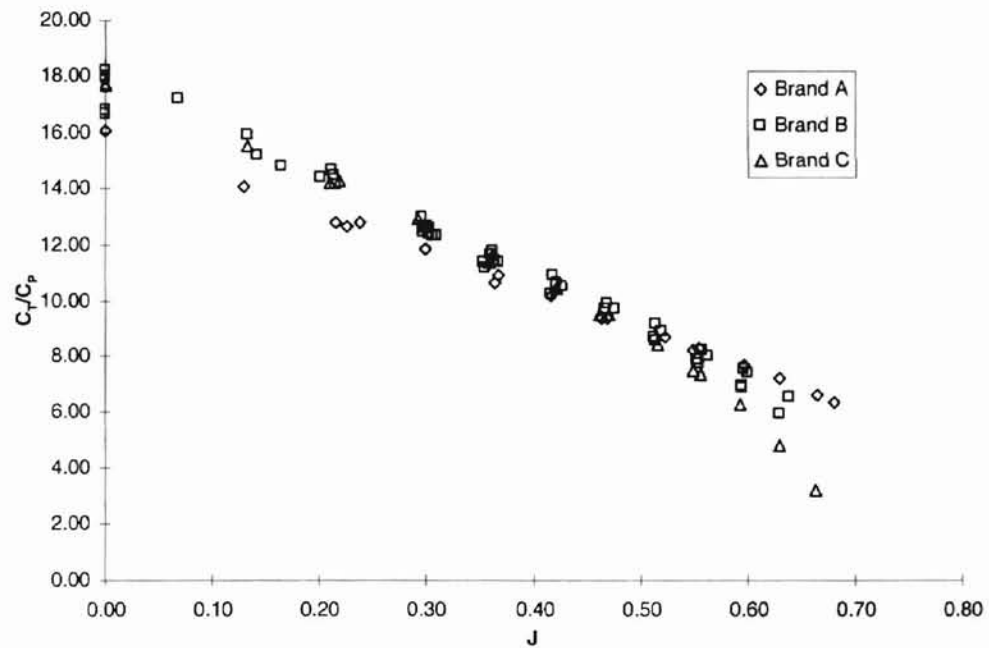


Figure 5.12 Differing Brand Effects on the Ratio of Thrust and Power Coefficient

5.4 Tip Clipping

The tip clipping investigation involves determining the effect of reducing the diameter of a given propeller. Not only does this change the diameter of the propeller it also changes the effective pitch as well. To determine the effect that this 'clipping' has on the propeller's performance a large diameter propeller was strategically selected so that after the diameter of this propeller had been reduced, it would now match the ratio of pitch to diameter of a second 'un-cut' propeller. The test was conducted at a fixed rotational rate of 7200 RPM while varying the tunnel speed from static to one inch of water.

The result of this investigation show that the 'clipped' propeller has all most double the thrust and power coefficients of the 'un-clipped' propeller, Figure 5.13 and Figure 5.14. However, it is the propeller efficiency curves, Figure 5.15, which are very interesting. While in all the previous investigation when both coefficients increased the overall efficiency of that given propeller fell by a noticeable amount, in this case the overall efficiency was only slightly less then the 'un-cut' propeller. The 'clipped' propeller had an overall peak efficiency of just over 79% and occurred at a higher advanced ratio of 0.70, where as the 'un-clipped' propeller had a peak efficiency of just under 81% and occurred at an advance ratio of 0.63.

The Figure 5.16 shows the overall effect of 'clipping' on the ratio of the thrust and power coefficients. Here even the effect on the static end of the curve can readily be seen. From the results, it can be seen that the 'clipped' propeller produces 18% less static thrust.

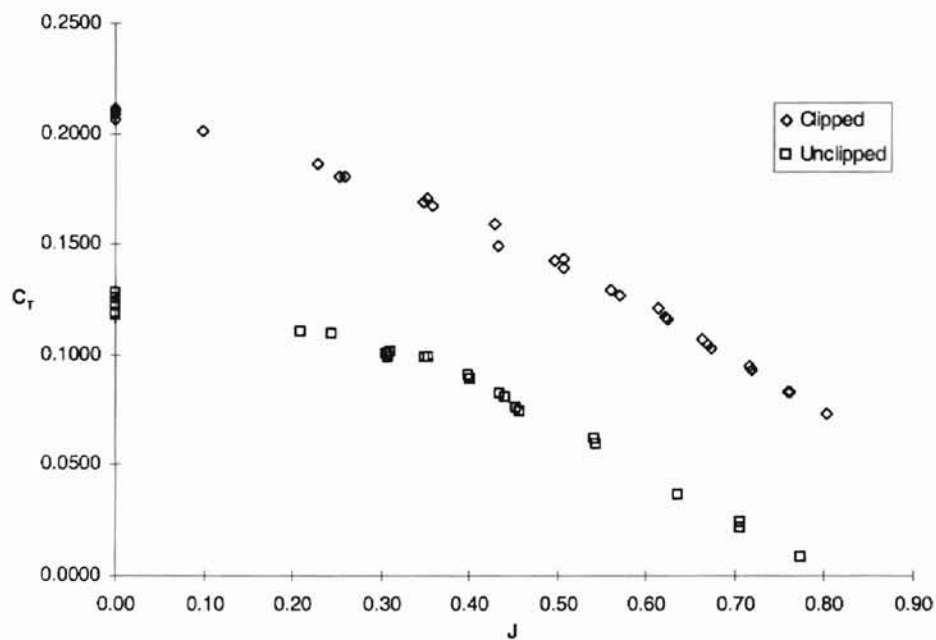


Figure 5.13 Tip Clipping Effects on the Thrust Coefficient

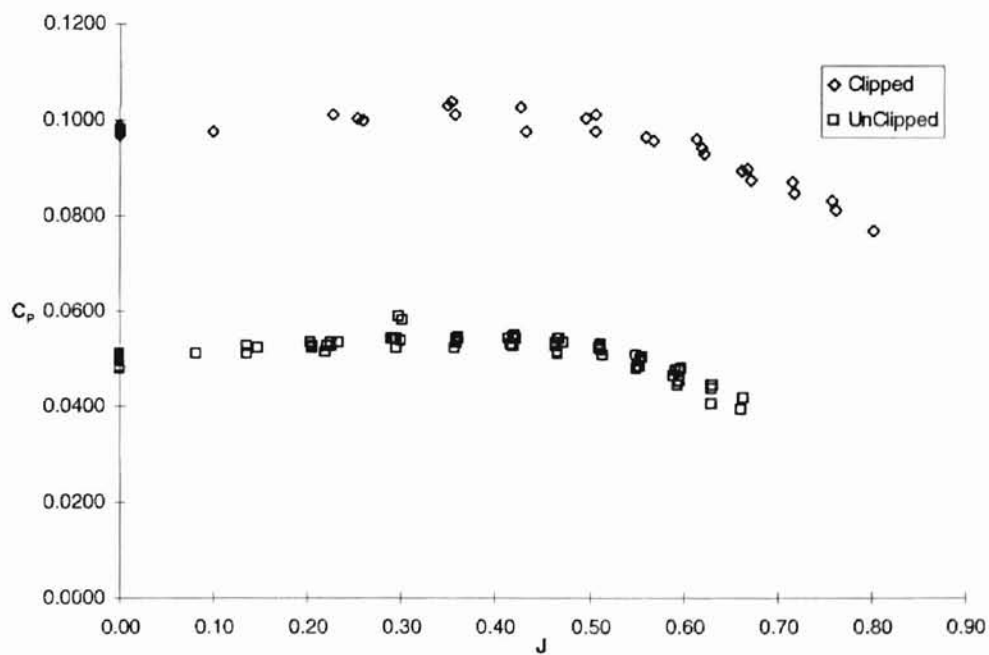


Figure 5.14 Tip Clipping Effects on the Power Coefficient

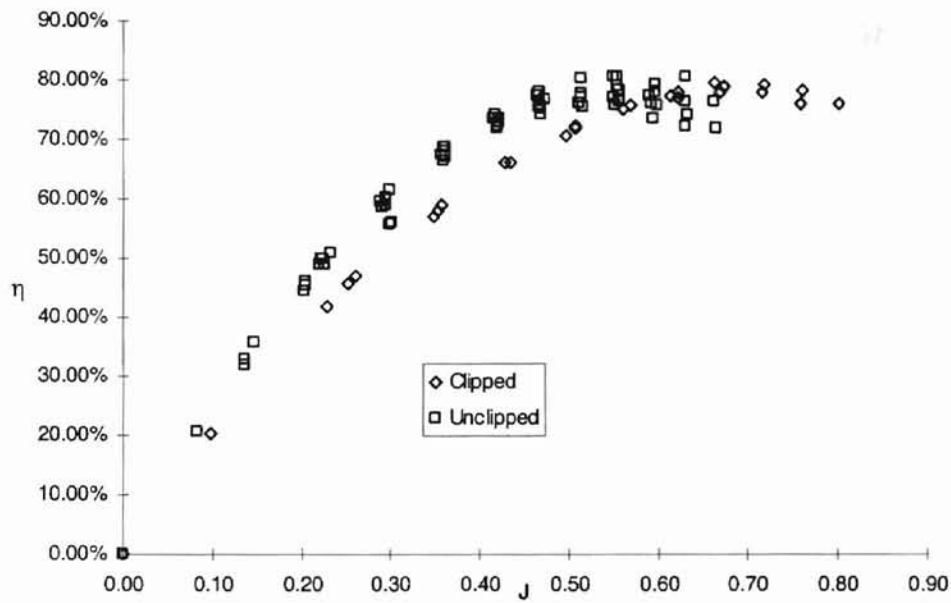


Figure 5.15 Tip Clipping Effects on the Propeller Efficiency

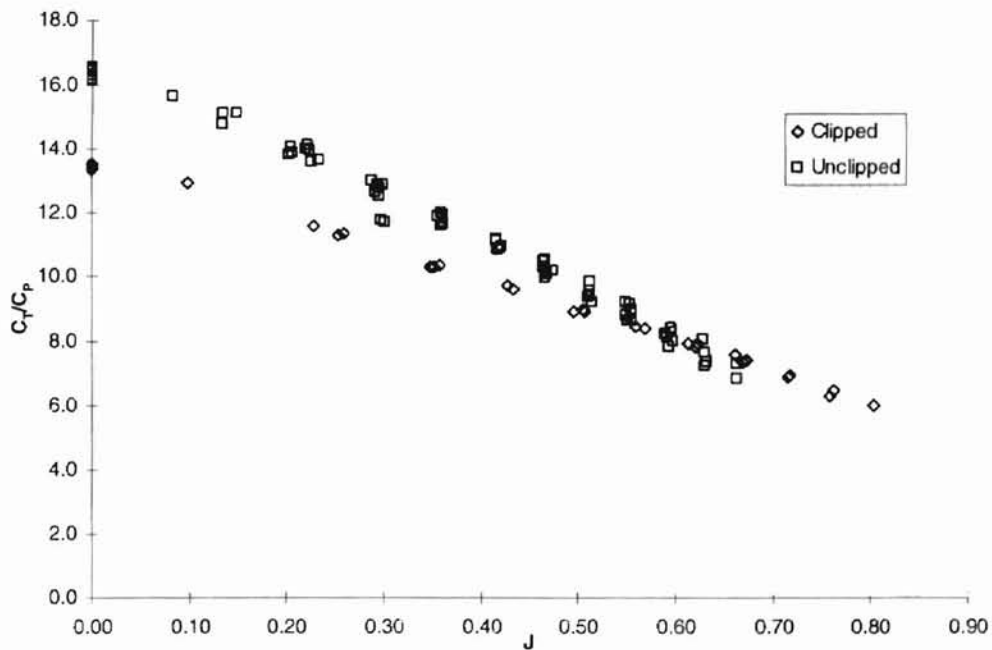


Figure 5.16 Tip Clipping Effects on the Ratio of Thrust and Power Coefficient

6 CONCLUSIONS AND RECOMMENDATIONS

6.1 Conclusion

A dynamometer has been developed that can be used to investigate the dynamic properties for small, 12" diameter, propeller at low Reynolds numbers. The system can be used to determine the thrust and torque coefficients as well as the overall propeller efficiency to within $\pm 2.5\%$. Thrust is found by measuring the strain produced by the deflection of two thin beams that support the entire device. The torque is measured by the strain produced by the twisting of a two-beam cruciform attached to a shaft. The shaft is then connected to the rear of the motor mount. The strain that is produced in both cases is measured by four strain gages that are attached directly to the beams. The strain gages are then connected in a circuit to form a full Wheatstone bridge, in which the output voltage corresponds to the thrust and torque placed upon the system. This voltage is then recorded on the computer by use of a data acquisition card and custom written program.

This dynamometer was then used conduct several experiments to determine the effect of several parameters on propeller performance, while varying the test section speed from static to one inch of water. All the experiments outlined in this thesis have shown how several parameters affect the actually dynamic propeller performance.

The first of parameters to be investigated was the effect of rotational rate. This investigated shows that there is little effect on propellers performance curves, even when the rotational rate is doubled. However, it did indicate that the static phase is effected by as much as 7% with a doubling of the rotational rate from 3600 to 7200 RPM.

The next parameter that was investigated was a family of curves produced by varying the pitch. The results obtained here can be used directly to aid in the design of a propulsion system for a remotely piloted vehicle, after one fits a curve to them. For they show that while you increase pitch the coefficients increase as well, and that there is a shift in both the peak efficiency and advance ratio.

The last two investigations were done to determine the effect of the geometry of the blade on the propeller's performance. This involved examining the effect of both tip clipping and how manufacturing brand type affected the performance. Both parameters appear to affect the thrust and torque coefficients, however the overall propeller efficiency does not appear to be overly effected. The only area where there does appear to be an effect is the static phase. Tip clipping a propeller produces 18% less static thrust than the thrust which is produced by an 'un-clipped' propeller of equal diameter.

All experiments conducted were done with the utilization of the low-speed wind tunnel facilities located in the Aerodynamics laboratory at Oklahoma State University. The typical time to conduct a single propeller performance investigation is under thirty minutes. This ability to quickly and accurately measure a single propeller's performance makes it easy and efficient for a propulsion system designer to not only obtain data for the design process, but then also to verify the design.

6.2 Recommendations

The following are recommendations that will aid in a decrease in the time required to analyze a given propeller arrangement or set of arrangements, or are areas that need to be further explored.

1. Automation of the tunnel velocity.
2. Include the rotational rate sensor in the automated data acquisition process.
Currently the user must enter this value by hand and then monitor the value during a run.
3. Investigation of the flow condition around the propeller at differing advance ratio with use of a high-speed camera and smoke for flow visualization around the blade. This should include both a change in advance ratio due to rotational rate as well tunnel velocity.
4. Investigate the performance of the propeller where the system is powered by a battery supply instead of the DC power supply.
5. Utilize Visual Basic to help 'streamline' the importation and processing of the raw data inside Excel.
6. Make use of a large dynamometer to investigate the effect of larger diameter propellers.

REFERENCES

- Abernethy, R.B., Benedict, R.P., and Dowdell, R.B., "ASME Measurement Uncertainty", Journal of Fluids Engineering, Vol. 107, June 1985, pp. 161-164
- Asson, K.M., "The Development of an Advanced Dynamometer System to Experimentally Determine Propeller Performance", M.S. Thesis, University of Notre Dame, Notre Dame, IN, 1990
- Bass, R.M., "Techniques of Model Propeller Testing", SAE Paper 83-0750
- Bass, R.M., "Small Scale Wind Tunnel Testing of Model Propellers", AIAA Paper 86-0392
- Borst, H.V., "Design and Analysis of Propellers for Low Reynolds Number Application to Mini-RPV's", SAE Paper 77-0999
- Foch, R.J. and Wyatt, R.E., "Low Altitude/Airspeed Unmanned Research Aircraft (LAURA) Preliminary Development" Aerodynamics at Low Reynolds Numbers International Conference Proceedings, Vol. III, 1986, 31.1-31.29
- Glauert, H., "The Elements of Aerofoil and Airscrew Theory", Macmillan Company, New York, 1943
- Harrison, G.L., "Measurement of a Counter Rotation Propeller Flowfield Using a Laser Doppler Velocimeter", AIAA Paper 87-0008
- Hurst, D.W., Methven, P.N. and Owen, D.T., "Wind Tunnel Testing of Small Scale Pressure Tapped Model Propellers" Aerodynamics 1986, 21.1-21.22
- Kline, S.J., "The Purposes of Uncertainty Analysis", Journal of Fluids Engineering, Vol. 107, June 1985, pp. 153-160
- Nelson, W.C., "Airplane Propeller Principles", John Wiley & Sons, 1944
- Mises, R.V., "Theory of Flight", Dover Publication, 1945
- Moffat, R.J., "Describing the Uncertainties in Experimental Results", Experimental Thermal and Fluid Science, 1988, pp. 3-17
- Schetz, J.A., Mallory, D.A. and Pelletier, D., "Numerical and Experimental Investigation of a Propeller Flowfield with a 3-D Non-Uniform Inflow", AIAA Paper 87-0607

- Takasawa, K. and Hashidate, M., "Design, Analysis and Experimental Verification of a Propeller Working in the Low Reynolds Number Range", Aircraft Symposium, 28th, Tokyo, Japan, Nov. 7-9, 1990, Proceeding, pp. 358-361
- Theodorsen, T. , " Theory of Propellers", McGraw-Hill, 1948

APPENDIX A

A Source Codes

A.1 PROPSCAN.CPP

```
#include "dl6.h"           // header file containing custom
                           // data acquisition routines
#include "airprops.h"      // header file for finding air properties
#define velslope 5.25     // Calibration Slope for Pressure Transducer

void main()
{
    int counter,sample,quit;
    float avgvolts,volt=0,avgvolts1,volt1=0,avgvolts2,volt2=0;
    float thrust=0,torque=0,vel=0,avgthrust,avgtorque,avgvel;
    float power,rps=1,velconv;
    FILE *output_file;

    clrscr();
    boardsetup();
    set_gain(1);
    chan_scan();
    velconv = airprops()*velslope; // determines Conversion Factor
                                   // per inch H2O
    printf("Torque 0   Thrust 1   Tunnel Vel 2 \n");
    printf("Enter number of sample to be taken:");
    scanf("%i",&quit);
    output_file = fopen("prop.dat", "w+");
    fprintf(output_file, "Tunnel Velocity\tRPS\tThrust\tTorque\tPower\n");
    fprintf(output_file, "Input\n");
    fprintf(output_file, "(ft/sec)\t(RPS)\t(mV)\t(mV)\t(Watts)\n");
    clrscr();
    printf("Enter RPS:");
    scanf("%f",&rps);

    while (rps >= 0)
    {
        for (sample=1; sample<=quit; sample++)
        {
            for (counter=1; counter<=1000; counter++)
            { /*
                volt += a2din()*(2./4095.)-1.;
                volt1 += a2din()*(2./4095.)-1.;
                volt2 += a2din()*(2./4095.)-1.;

                avgvolts=volt/counter; // Torque
                avgvolts1=volt1/counter; // Thrust
                avgvolts2=volt2/counter; // Tunnel Velocity */
            }
            gotoxy(7,10);
            printf("%8.0f Torque %17.0f Thrust/Drag\n",avgvolts*1000,avgvolts1*1000);
            printf("%14.3f Tunnel Pressure %8.2f Tunnel Velocity\n"
```

```

        ,avgvolts2, (floor(avgvolts2*1000)/1000)*velconv);

    thrust += avgvolts;
    torque += avgvolts1;
    vel += avgvolts2;
    volt=0; volt1=0; volt2=0;
}

avgthrust = thrust/sample; avgtorque = torque/sample;
    avgvel = vel/sample;
    clreol();
    printf("Enter Input Power (Watts):");
    scanf("%f",&power);
    fprintf(output_file, "%5.2f\t%5.2f\t%5.0f\t%5.0f\t%5.0f\n "

        ,floor(avgvolts2*1000)*(velconv/1000),rps,avgthrust*1000,
        avgtorque*1000,power);

gotoxy(1,1);

    thrust = 0; torque = 0; vel = 0;
    printf("Last RPS:%8.2f",rps);
    printf("\nEnter RPS:");
    clreol;
    scanf("%f",&rps);
}
}

```

A.2 D16.H

```

#define BASEADR 0x330
#define A2DLSB  BASEADR + 0
#define A2DMSB  BASEADR + 1
#define CHANREG  BASEADR + 2
#define DIO      BASEADR + 3
#define D2A0LSB BASEADR + 4
#define D2A0MSB BASEADR + 5
#define D2A1LSB BASEADR + 6
#define D2A1MSB BASEADR + 7
#define STATREG  BASEADR + 8
#define CTRLREG  BASEADR + 9
#define CNTRENABLE BASEADR +10
#define GAINREG  BASEADR + 11
#define CNTR0    BASEADR + 12
#define CNTR1    BASEADR + 13
#define CNTR2    BASEADR + 14
#define CNTRCTRL BASEADR + 15
#define VREF     5.0
#define CLOCK    10000000
#define DEBUG 0 // 1 is on 0 is off

#include <conio.h>
#include <dos.h>
#include <math.h>

```

```

#include <stdio.h>
#include <values.h>
#include "bitprint.h"    //Displays ports as a binary number

void boardsetup();
void set_gain(int);
void sng_chan(int chan);
void timer_values(float freq,unsigned int *n1,unsigned int *n2);
void set_timer(unsigned int n1,unsigned int n2);
void chan_scan();
int lo(unsigned int);
int hi(unsigned int);
int a2din();
void aout0(float voltage);
void aout1(float voltage);

int i;
int total_chan;

void boardsetup()
{
    outportb(CTRLREG,0x0);
    outportb(CNTRENABLE,0x0);
    outportb(STATREG,0x0);
    outportb(CNTRCTRL,0x30);
    outportb(D2A0LSB,0x00);    // Analog Out Channel 0
    outportb(D2A0MSB,0x00);    // Reset to Zero
    outportb(D2A1LSB,0x00);    // Analog Out Channel 1
    outportb(D2A1MSB,0x00);    // Reset to Zero
}

void sng_chan(int chan) // Single Channel Scan
{
    int muxscan;
        muxscan=(chan <<4)+chan;
        outportb(CHANREG,muxscan);
}

void chan_scan() // Multi-Channel Scan
{
    int lowerchan,upperchan,muxscan,muxsetting;

    printf("\n %s","Input lower channel to scan (0-7):");
    scanf("%d",&lowerchan);
    printf("\n %s","Input upper channel to scan (0-7):");
    scanf("%d",&upperchan);
    muxscan=(upperchan <<4)+lowerchan;
    printf("\n");
    outportb(CHANREG,muxscan);

    if (upperchan >= lowerchan)
        total_chan = (upperchan-lowerchan)+1;
    else {
        printf("\a%s",
            "Error Lower channel is greater than upper channel");
        chan_scan();
    }
}

```

```

}

void set_gain(int gain) // gain setting 0 +10, 1 +1, 2 +0.1, 3 +0.02
// Can differ for each channel
{
    outportb(GAINREG, gain);
}

int a2din() // Analog to Digital Input
{
    int eoc, lsb, msb;
    int datavalue;

    outportb(A2DLSB, 0x10); // Start A/D Conversion
    do
    {
        eoc=inportb(STATREG);
    } while ((eoc>>7) != 0);
    lsb=inportb(A2DLSB);
    msb=inportb(A2DMSB);
    datavalue=(msb*16)+(lsb>>4);
    // current_channel=lsb & 0x0F;
    // next_channel=inportb(STATREG) & 0x0F;
    return(datavalue);
}

void aout0(float voltage) // Analog Out Channel 0
{
    unsigned int datavalue;

    datavalue = ceil(voltage*(4095.0/VREF));
    datavalue = datavalue << 4;
    if(DEBUG)
    {
        printf("\nDatavalue0:%u", datavalue);
        printf("\nVoltage0:%f", voltage);
    }
    outportb(D2A0LSB, lo(datavalue));
    outportb(D2A0MSB, hi(datavalue));
}

void aout1(float voltage) // Analog Out Channel 1
{
    unsigned int datavalue;

    datavalue = ceil(voltage*(4095.0/VREF));
    datavalue = datavalue << 4;
    if( DEBUG)
    {
        printf("\nDatavalue1:%u", datavalue);
        printf("\nVoltage1:%f", voltage);
    }
    outportb(D2A1LSB, lo(datavalue));
    outportb(D2A1MSB, hi(datavalue));
}

void timer_values(float freq, unsigned *n1, unsigned *n2)

```

```

// Find the two 16 bit numbers for the 8254 Counter
{
    unsigned maxint=65535; // 16 bit number is the max
    float cn1=1.0,cn2,tcn1,tcn2=1.0,flag1=1.0,flag2=1.0,oldflag=1.0,
        divisor;

    divisor=CLOCK/freq;
    while (flag1 != 0)
    {
        cn1++;
        cn2 = divisor/cn1;
        flag1 = cn2 - floor(cn2);
        if (cn2 > maxint) flag1 =1;
        if (cn1 >= maxint) flag1 =1;
        if (flag1 <= oldflag)
        {
            oldflag = cn2 - floor(cn2);
            tcn1=cn1;
            tcn2=cn2;
            flag2=1;
            if (floor(cn2) <= 2) flag1=0;
        }
    }

    if (flag2)
    {
        cn2=tcn2;
        cn1=tcn1;
    }

    *n2=cn2;
    *n1=cn1;
    if (DEBUG)
    {
        printf("Timer Values \t%u\t%u\n",*n1,*n2);
        printf("Frequency %8.5f\n",CLOCK/(cn1*cn2));
    }
}

void set_timer(unsigned int n1,unsigned int n2) // Set 8254 Counter
{
    outportb(CNTRCTRL,0xB4);
    outportb(CNTRCTRL,0x74);
    outportb(CNTR2,lo(n2)); // Send LSB to Counter 2
    outportb(CNTR2,hi(n2)); // Send MSB to Counter 2
    outportb(CNTR1,lo(n1)); // Send LSB to Counter 1
    outportb(CNTR2,hi(n2)); // Send MSB to Counter 1
    if (DEBUG) printf("Set Timer \t%u\t%u\n",n1,n2);
}

int lo(unsigned int i) //return the low bytes of a 16-bit number
{
    return((i-hi(i)*256));
}

int hi(unsigned int i) // return the high bytes of a 16-bit number

```

```
{
return(i>>8);
}
```

A.3 AIRPROPS.H

```
#define gravity 9.80665
#define rhohg 13595
#define rhoh20 998
#define R 287
#define S 110.4
#define B 1.458E-06

float airprops();
float airprops()
{
    float bar,atmpress,airtemp,rhoair,velcon,dvisc;
    printf("Enter Corrected Barometer Reading:");
    scanf("%f",&bar);
    printf("\nEnter Tunnel Temperature:");
    scanf("%f",&airtemp);
    atmpress = gravity * rhohg * bar / 1000;

    // Ideal Gas Law to find density of air
    rhoair = atmpress / (R * (airtemp + 273.15));

    // Conversion between inches of H2O and Velocity
    velcon = sqrt(2*gravity*rhoh20*0.0254/rhoair);

    // Sutherland Equation for Dynamic Viscosity
    dvisc =(B * sqrt(airtemp + 273.15))/
        (1 + (S/(airtemp + 273.15)));

    // Covert to English Units
    dvisc = dvisc/1.488164;
    rhoair = rhoair/16.01846;
    velcon = velcon/0.3048;

    return(velcon);
}
```

A.4 BITPRINT.H

```
#include <limits.h>

void bit_print(int);
void bit_print(int value)
{
    int i;
    int n = sizeof(int) * CHAR_BIT ;
    int mask = 1 << (n-1);
    printf("\n");
    for(i=1; i <=n; ++i)
    {
        putchar (((value & mask) == 0) ? '0' : '1');
        value <<=1;
        if (i % CHAR_BIT == 0 && i <n)
            putchar(' ');
    }
}
```

VITA

Joseph Conner Jr.

Candidate for the Degree of

Master of Science

Thesis: LOW COST DYNAMOMETER SYSTEM TO EXPERIMENTALLY
MEASURE PROPELLER PERFORMANCE AT LOW REYNOLDS
NUMBERS.

Major Field: Mechanical Engineering
Specialty Field: Aerospace Engineering

Biographical:

Personal Data: Born in Tulsa, Oklahoma, On December 31, 1970, the son of
Joseph Conner and Sandy Conner.

Education: Received Bachelor degree in Aerospace Engineering from Oklahoma
State University, December 1995. Completed the requirements for the
Master of Science degree with a major in Aerospace Engineering at
Oklahoma State University in December, 2000